1

In-Situ TEM

1.1 Introduction

Transmission electron microscope (TEM) and related techniques (scanning transmission electron microscope [STEM], tomography, holography, Lorentz microscopy, etc.) are preferred methods to understand the atomic-scale structure and chemistry of materials, especially for nanomaterials. The size of grains, grain boundary structure, density of defects, dislocations, etc. control the materials properties making such information critical for their synthesis and applications. Beautiful atomic resolution images, electron diffraction patterns, and chemical maps provide unprecedented information about the structure and chemistry of the defects and grain boundaries in the material under investigation. Commonly employed procedure is to characterize the starting material (prenatal) and end products (postmortem) to deduce the pathway for chemical reactions or phase transformations occurring when the material is subjected certain stimuli, such as temperature, pressure, and/or mechanical stress. Main motivation behind this exercise is to be able to generate synthesis–structure–property relationships by identifying structure and chemistry of materials formed under different synthesis conditions and measuring their properties.

In-situ TEM observations provide a direct visualization of structural and chemical changes under synthesis or operational conditions of nanomaterials when they are subjected to relevant external stimuli. Note that (i) TEM requires thin samples such that most of electrons are transmitted through after interacting with the sample, (ii) we need high vacuum to avoid electron scattering by the gas molecules, (iii) electrons can be treated as particles and/or waves, (iv) image formation optics is quite similar to light microscopes. The restrictions imposed by first two points require us to find methods to make thin electron transparent samples and modify the TEM column or sample holder, to accommodate required experimental conditions. We will address these requirements in this book as described below.

> Seeing is believing but feeling is the truth.
>
> – Thomas Fuller

In-Situ Transmission Electron Microscopy Experiments: Design and Practice, First Edition. Renu Sharma.

1.2 General Scope of the Book

During past couple of decades, materials word is continuously shrinking in size where the size of semiconductor chips or batteries has dropped down to nanometers. As a result, fabrication methods have adapted from synthesizing building blocks for future assembly to combining synthesis and assembly process into one step, putting stringent control on the fabrication process.

Therefore, TEM-based techniques have become a method of choice to understand and predict the desired synthesis or fabrication route for materials with desired properties. TEM community has recognized this need and responded accordingly. There has been an explosion in the breadth of combinatorial in-situ TEM techniques that are now readily available due to advanced microscope controls, the development of microfabricated TEM sample holders, and automated data handling. Moreover, monochromated electron source and aberration-corrected lenses have made it possible to use medium-voltage microscope (200–400 keV TEM) with a pole-piece gap of 5 mm to 7 mm, needed for inserting TEM holders equipped with heating, cooling, biasing, mechanical testing, liquid and gas containment, etc. for atomic-scale structural and chemical characterization. These advancements and rapidly changing demand have attracted many more scientists to participate in the field, with or without formal training for employing TEM platform for performing experiments. As a result, a symposium or session (sometimes more than two) on the in-situ TEM characterization is included in most of the major conferences in chemistry and materials field (American Chemical Society (ACS), American vacuum Society (AVS), Materials Research Society (MR S), American Institute of Chemical Engineers (AIChE)), beyond microscopy and microanalysis (M&M), and the number of publications has increased exponentially (Figure 1.1).

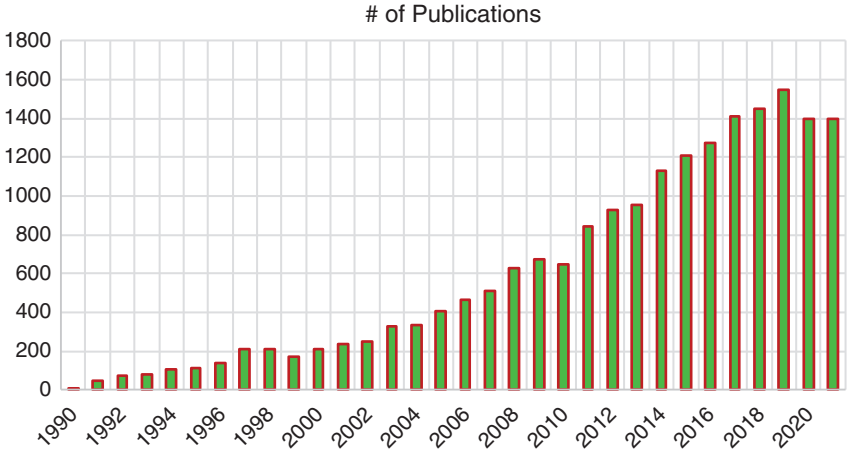

Figure 1.1 Number of publications reporting results obtained using in-situ or operando techniques in the last 40 years. Note the exponential growth since 2010. Source: Data from Web of Science.

1.3 Why In-Situ TEM

> Going from pretty pictures to touching and feeling
>
> – Murray Gibson

Let us first understand the meaning and difference between two commonly used terms: "in-situ" and "operando." First term "in-situ TEM" that we will commonly use throughout this book is also valid for in-situ STEM, in-situ analytical transmission electron microscope (ATEM) (EDS or EELS), etc. "In-situ" originates from Latin that means "in place" or "in position" and is used in many contexts. For us, it means TEM characterization of materials subjected to external stimuli at a specific "position or place" under synthesis or functioning conditions. Examples of external stimuli include, but are not limited to, temperature, gas or liquid environment, electrical biasing, magnetic or mechanical force, etc. to the material under observation using TEM-based platform. The term "operando" also originates from Latin and means "working," for example, we refer to the term in context of measuring the reactants, the product, and/or functionalities under working (functioning) conditions. In simple terms, while "in-situ" observations provide information about the changes under specific environmental conditions, the "operando" implies measuring the consequence of these conditions. In catalyst community, operando is strictly used to measure the kinetics as function of reaction variables, such as composition of reactants, products, nature (including loading, size) of catalyst/support, temperature, and pressure. Although in-situ TEM experiments have unveiled several catalytic mechanisms at atomic scale, most of the time, we do not operate under "working" reactor condition.

These are not strict definitions but are generally used by the materials, physical, and chemical scientists. In-situ TEM observations are more frequently used to follow reactivity of the material; however, operando measurements are relevant for catalysis, battery operations, and nanomaterial synthesis. Also, we generally use the term "in-situ" or "operando" when pursuing the changes with time, that may be termed as dynamic changes. In-situ characterization and measurements have following advantages:

- Same area or same nanoparticle is observed before, after, and during the reaction process such that all steps, including intermediate steps (if any), are identified.
- A careful design of the experiments leads to the observation and understanding of the relationship between morphological, structural, and chemical changes concurrently.
- Both the thermodynamic and the kinetic data of the reaction process may be obtained at nanometer or sub-nanometer scale.
- In-situ observations result in considerable time saving as the synthesis, property measurement, and characterization can be performed simultaneously.
- In-situ correlative light and electron microscopy (CLEM) is used to combine nanoscale and microscale characterization of the same sample subjected to same experimental conditions.

However, in-situ TEM experiments have their limitations and will be discussed later (Section 1.7).

1.4 TEM: Overview

This section is a brief reminder of some of the simple facts about the functioning of the TEM/STEM instruments. References to the books and articles are provided at the end of the chapter and should be consulted for detailed understanding of the electron optics, image formation, and chemical analysis.

1.4.1 Historical Perspective

After the advent of using coaxial magnetic coils to focus electron beam to a point, Ernst Ruska and Max Knoll, in 1931, built and demonstrated the first TEM, capable of magnifying objects to approximately 400 times, demonstrating the principles of electron microscopy [1]. The resolution limit of electron microscopes increased rapidly and, in 1939, and Siemens introduced first commercial instrument based on Ruska's design. Further development in the resolving power was slow, but a number of research groups worked on developing their own instruments leading to the formation of a number of commercial companies that took over the market from Siemens. Since then, there has been a steady development in improving the image as well as energy resolution. Moreover, several other applications that take advantage of the electron interaction with the sample such as diffraction and chemical analysis (energy-dispersive X-rays [EDS], electron energy-loss spectroscopy [EELS], cathodoluminescence [CL], etc.) have also been developed. To continue to take advantage of the TEM platform for in-situ observations, it is imperative for us to understand the principles of electron scattering and image formation in a TEM, basic design of TEM/STEM/ATEM instruments, and appreciate the developments over last 90 years that resulted in commercially available modern microscopes.

1.4.2 Electron–Sample Interactions

Electron–sample interactions can be divided into two main categories, elastic and inelastic (Figure 1.2). The collision of incident electrons with the nucleus is scattered by larger angles that results in the elastic scattering, whereas inelastic electrons scattering results from the collision of incident electron with the electrons cloud around the nucleus, including inner shell electrons, and is limited to small angles or small energy losses (below 50 eV). The elastic scattering contributes to the phase change in the transmitted electrons and is important for image formation as it contributes to the image contrast. In simple terms, elastic scattering allows us to acquire diffraction and images from the sample.

Apart from elastically and inelastically scattered electrons, the electron–sample interactions result in generating a host of signals, such as electron–hole pairs, back-scattered electrons, secondary electrons, Auger electrons, characteristic X-rays, and visible light (Figure 1.2). While secondary and back-scattered electrons are generally not used during TEM characterization, they are important for scanning electron microscope (SEM). We also ignore Auger electrons, but the light generated as a result of electron–hole recombination, i.e. CL, is often used to understand the semiconducting properties in materials. EELS and characteristic X-ray signal (EDS) are routinely used to obtain chemical composition of the sample.

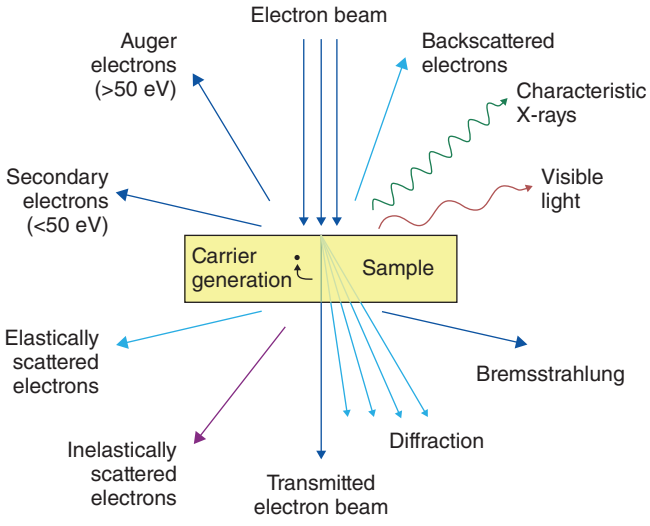

Figure 1.2 Distinct signals generated due to elastic and inelastic interactions of electrons with the sample. Most of the TEMs are equipped to collect electron diffraction, image, EELS and EDS data.

1.4.3 Overview of Modern TEM

Let us now revisit the ways TEMS/STEM instruments enable us to collect some or all the signals generated as a result of the electron/sample interaction shown in Figure 1.2. Image formation in TEM is based on the same optical principles as for a light microscope. The difference is that in a TEM, the electrons are used as a source of light and magnetic lenses are used for image formation and magnification. TEM can stand for transmission electron "microscope" or "microscopy," where one is an instrument (noun) and the other is a technique (adverb). For simplicity's sake, we will use the same acronym for both. We assume that the placement of the acronym in a sentence should be obvious enough to distinguish between "microscope" and "microscopy." Also, we use TEM for the basic system and specialized instruments or techniques, such as STEM or ATEM, can be considered as extension of the basic system. Although we will see that this simple explanation is not entirely correct as their design and functioning could have noticeable differences, i.e. a dedicated STEM has different optics than a TEM and an ATEM may have larger objective pole-piece gap. Here we will concentrate on TEM/STEM instruments as they are most effective for in-situ experiments. Figure 1.3a shows a simple ray diagram and location of various components of a basic TEM, and Figure 1.3b shows the detailed features of a modern double-corrected (C_s) TEM. A detailed description and functioning of each component are described in Sections 1.4.3.1–1.4.4.

1.4.3.1 Electron Source or Electron Gun

Electron gun can be considered as an "illumination source" for samples under observation and is an important component. High-energy electrons can be extracted from a thermoionic source such as a tungsten filament, or LaB_6 crystal, or field

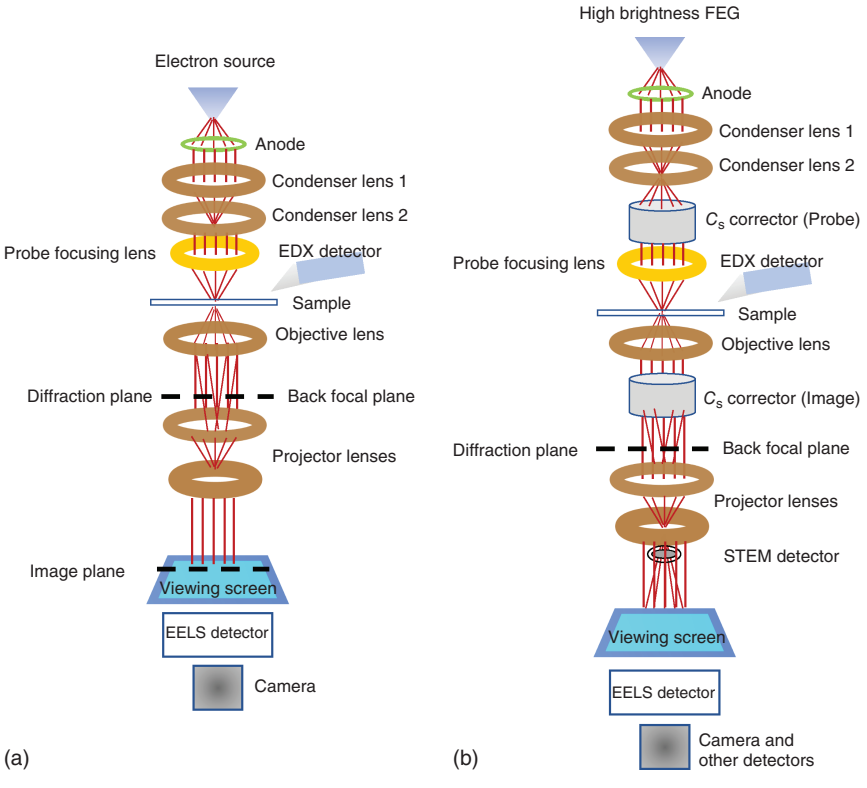

Figure 1.3 A schematic illustration of various components of (a) basic TEM and (b) double-corrected modern TEM/STEM with EDS, EELS, and STEM detectors.

emission from a pointed tungsten or tungsten tip coated by ZrO_2. Electrons are emitted from thermoionic sources by heating the source to a very high temperature. Electron density, brightness, coherence, and energy resolution of the illumination system are controlled by the electron source. Whereas thermoionic sources are easy to make and operate, they have low electron density, brightness, energy resolution and are incoherent. A field-emission source/gun (FEG) provides high brightness, energy resolution, and coherence, where the electrons are extracted from the source by applying an electric field either at room temperature (cold FEG) or at high temperature (Schottky). Simple but detailed information about the sources and their properties can be found in Chapter 5 of Ref. [2]. Moreover, small probes, on the order of sub-nanometer, can be formed using a FEG, which determines the spatial resolution for STEM imaging and atomic-scale chemical mapping [3].

> The type of electron gun is decided while constructing the microscope and cannot be changed afterward as the gun chamber, extraction and focusing systems are designed for specific source and are not easily interchangeable.

1.4.3.2 Lenses

Lenses are needed to focus the electrons on the sample and on the image screen after passing through the sample. In 1927, Busch successfully focused the electrons using electromagnets that motivated Ruska to design the first microscope in 1931 [1]. The same principle is used even today to construct lenses, where the magnetic field is generated by passing current through coils wound around a soft magnetic core. Since the magnetic field strength within the lens is function of current flowing through the electrostatic coils, both the focal length and the focal point can be controlled by varying the current. Following are the lenses used in a TEM:

I. **Condenser lens:** This lens is used to focus the beam of electrons, emitted from the gun to a point on the sample such as to form a point source. Modern TEMs have a set of condenser lenses that can be used to control the probe size and location of crossover along the optical axis.
II. **Objective lens:** Objective or image forming lens is located around the sample and focuses the transmitted electron beams on the image plane. The magnetic assembly generally consists of two parts, commonly known as pole pieces, placed above (top) and below (bottom) the sample, and is the most critical component that produces an axially symmetric magnetic field. The sample is located between these two pole pieces, collectively called objective lens, and defines the image resolution of the microscope. For optimum performance, the sample should be located at a specific position, called "eucentric height" between the two pole pieces. The gap between the pole pieces determines:
    - The achievable tilt angle of the holder tip, which is important, (i) to align the sample along one of the crystalline zone axes parallel to the incident beam, (ii) to collect highest X-ray signal for chemical analyses, and (iii) to obtain 3D images using tomography.
    - The space to insert objective aperture (OA) in the back focal plane of the sample or a CL detector.
    - The location of the sample within the gap for optimum resolution.

    Note that objective lens is probe forming lens in STEM mode for a TEM/STEM instrument, thus also determines the image resolution in STEM mode.
III. **Projector or magnifying lens:** Keep in mind that image resolution is determined by the objective lens and cannot be improved by employing other lenses; however, they can be used for image magnification that helps us see subtle changes in the image contrast. A set of electromagnetic lenses, known as projector lenses, provide this magnification. We can collect diffraction patterns or images by switching between image plane and back focal plane.

1.4.3.3 Lens Aberrations

Electromagnetic lenses, used to focus electrons, suffer from similar aberrations as the optical lenses, albeit they arise from different reasons. Spherical aberrations arise due to difference in the angle subtended by the electrons arriving at the lens from the electron source (for condenser lens) or from the sample (for objective lens). Electrons leaving a point object at large angle are scattered too strongly by the lens and brought

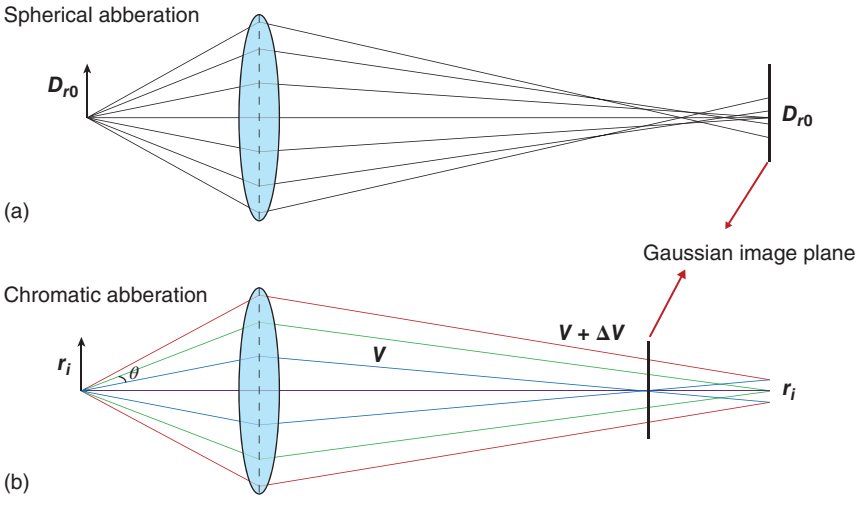

Figure 1.4 Simple ray diagrams showing the origin of spherical (a) and chromatic (b) aberrations.

to focus before the Gaussian plane giving rise to disc of confusion (Figure 1.4a). The diameter of the Gaussian image formed by point thus is given by

$$\delta = C_s\theta^3 \tag{1.1}$$

where C_s is spherical aberration constant. The third-order dependence on θ implies that the beams scattered at high angles are most affected by aberrations. On modern instruments, the C_s ranges about 0.4 and 2.5 mm and can be corrected by using appropriate optics as will be explained under Section 1.4.3.4.

On the other hand, electrons with varying energy, ΔV, will also be focused on different points due to the small variation in the wavelength, which is the source of chromatic aberration (Figure 1.4b). It is important to note that modern high-voltage tanks, used to generate electrons, are very precise but not perfect. Following are the three important sources of fluctuation in the wavelength/voltage of the electrons:

- The energy spread of the electron leaving the filament.
- High voltage instabilities (typical $\Delta V_o/V_o$ is 2×10^{-6}/min; V_o is the operating voltage of the microscope).
- Varying energy losses in the specimen.

Currently, both aberrations can be corrected using a set of lenses that generate negative C_s or C_c such as the positive values of imaging lenses are canceled out. A monochromator is also employed to mitigate the energy spread of the electrons leaving the filament. As expected, achievable image and energy resolution of such microscopes is at sub-nanometer and below 1 eV, respectively.

Astigmatism Just as for optical lenses, a deviation from perfect circularity is commonly present for electromagnetic lenses and could be due to imperfections in the iron core, machining error, asymmetrical windings, dirty apertures, etc. As a result, a stretching in the image is observed as a point object is focused. This problem can be

easily recognized by changing the focus as the stretching direction will change going from under focus to overfocus. Most microscopes are equipped with individual stigmator coils for all lenses to compensate for this distortion. Modern microscopes with aberration correctors also provide a precise correction of astigmatism for condenser and/or objective lenses.

> The lenses in a TEM have similar aberrations as optical lenses, but most of them can be corrected.

1.4.3.4 Aberration Correctors

Both the image and spectrum resolution are affected by the lens aberrations in a TEM [4–6]. Apart from C_s and C_c, described above, the energy of all electrons hitting the sample may not be the same, i.e. electron beam is not monochromatic. The high-voltage tank of most microscopes is designed to keep the energy fluctuation to a minimum value, and some sources are equipped with a monochromator. There are a number of ways, such as using electrostatic energy filter [7], or using a combination of electrostatic and magnetic quadruples [8], to filter out electrons with higher energy spread but often results in loss of intensity of the source. The energy resolution of a monochromated source may vary from 8 to 80 meV. We also find that the image resolution is also improved by using a monochromated source.

A TEM with C_s and C_c corrector for objective lens is also readily available [9, 10]. Both the cost and height of the TEM column increase with incorporation of correctors (Figure 1.3b).

1.4.4 Data Acquisition Systems

Electron–sample interactions result in generating various imaging and spectroscopy data that need to be collected for further analysis and documentation. Modern microscopes use digital cameras to record images, videos, diffraction patterns, EDS and EELS data. A microscope can be equipped with different digital detectors for recording TEM, STEM, annular dark-field (ADF), or bright-field (BF) images, or spectroscopy data such as EELS, EDS, or CL. We will look at them in detail as we work out the experimental plans.

1.4.4.1 Types of Detectors

Recording medium for image, DP, and spectroscopy data has different requirements. Whereas spectroscopy data have always been acquired using digital detectors, photographic film or image plates were used for recording images and DP due to their high dynamic range (pixel resolution) in the past. We should keep in mind that although recording medium to acquire DP and images may be the same, the acquisition process and time is different due to different intensity range present in the signals. The films have recently been replaced by electronic media such as phosphor/photomultiplier (PMT) or fiber-optic charge-coupled device (CCD). Here the phosphor is used as a scintillator to convert electrons into photons that are then

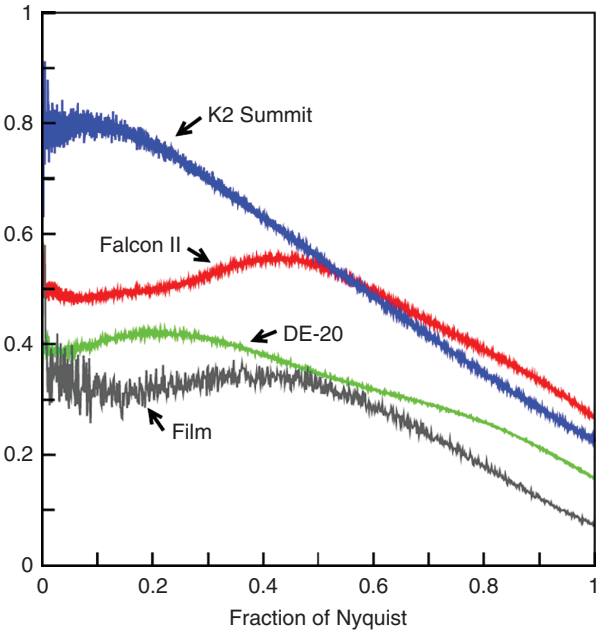

Figure 1.5 Measured DQE as a function of spatial frequency for the DE-20 (green), Falcon II (red), and K2 Summit (blue). The corresponding DQE of photographic film is shown in black. Source: McMullan et al. [13]/Elsevier/CC BY-3.0.

detected by a PMT or a CCD. PMT could be preferred for in-situ measurements due to their faster acquisition time, but their performance, as measured by their detective quantum efficiency (DQE), reduces at higher operating voltages (>120 keV) making CCD a better option. With continued rapid improvement in technology, a high DQE $\approx$ 0.7 and faster acquisition rate can be achieved for medium-voltage microscopes (200–300 keV) [11] by using direct electron detectors (DEDs) equipped with monolithic active pixel sensors. Furthermore, digital data acquisition enables data processing, including drift correction and adding a few frames to improve signal-to-noise ratio to obtain atomic resolution images at high time resolution [12]. The digital images are also compatible with machine learning approaches that improve our ability for unambiguous data analysis (Chapter 9). Figure 1.5 shows a comparison between three commercially available DED cameras and photographic film [13].

Apart from the DQE, time resolution, often termed as temporal resolution, is an important factor for in-situ measurements. Ideally, we need both high spatial and temporal resolution to decipher metastable steps of a chemical or physical process under investigation. Currently, ms time resolution is possible using DED cameras or another technology based on "pump and probe" idea (see Section 1.6.3). CMOS camera with scintillator [14] and pixel array detector [15] are a few other types of detectors available, and technology is improving at a fast pace, and cameras with both high spatial and temporal resolution are available for in-situ measurements.

1.5 TEM/STEM-Based Characterization Techniques

As we mentioned earlier, we assume that the readers of this book have thorough knowledge and adequate experience to operate TEM/STEM instruments. This section is a rapid review of TEM-based techniques that are available for in-situ measurements.

1.5.1 Diffraction

Electron diffraction is formed in the back focal plane of the objective lens and provides following structural information:

- **Crystallinity:** Diffuse rings in a DP indicate that the sample is amorphous (Figure 1.6a), spots on a ring pattern indicate polycrystalline nature (Figure 1.6b), and a 2D spot pattern is indicative of a single crystal (Figure 1.6d).
- **Structure of crystalline sample:** A single crystal sample can be aligned along one of its crystallographic zones to obtain structural information using selected area electron diffraction (SAD or SAED), convergent beam electron diffraction (CBED) (Figure 1.6e), nanobeam electron diffraction (NBED or NED), or nano area electron diffraction (NAED) (see below for details).
- **Defects:** A streaking or faint lines along the spot patterns (Figure 1.6c) indicate the presence of defects in the structure, which can then be further investigated using imaging.
- **Long-range order:** Presence of faint spots, or satellite spot, along with stronger spots, indicates the presence of long-range order along one of the crystallographic directions or perpendicular to viewing direction, respectively (Figure 1.6f).
- **Strain:** presence of faint lines along 2D diffraction spots is indicative of the presence of strain in a single crystalline sample. A number of methods to analyze and measure strain from electron diffraction patterns, especially from CBED or NBED, have been developed [17–19].

We often use a parallel electron beam and place an aperture, i.e. selected area aperture, to form diffraction pattern from a desired area (SAED or SAD). Such DP provides us information about the crystallinity and orientation of the sample. Some of the structural information, such as *d*-spacing and angle between planes in projection, is also obtained from these patterns. We can select the diffracted beams, using an objective aperture (OA) we want to use to form an image. For example, outer most diffraction spots arise from multiple scattering events, so we can improve image contrast by discarding them. We can also select one or two diffraction spots and discard central beam to form dark-field TEM image.

A CBED, which is in form of discs instead spots (Figure 1.6e), provides detailed structural information, such as crystal class and symmetry. Methods have been developed to use a CBED pattern to determine crystal structure by removing contribution of inelastically scattered electrons [20]. Nowadays, we can converge electron beam to nanometer size to obtain diffraction pattern from nanometer-size area, NBED or NED [21]. Interestingly, modern microscopes also allow us to obtain

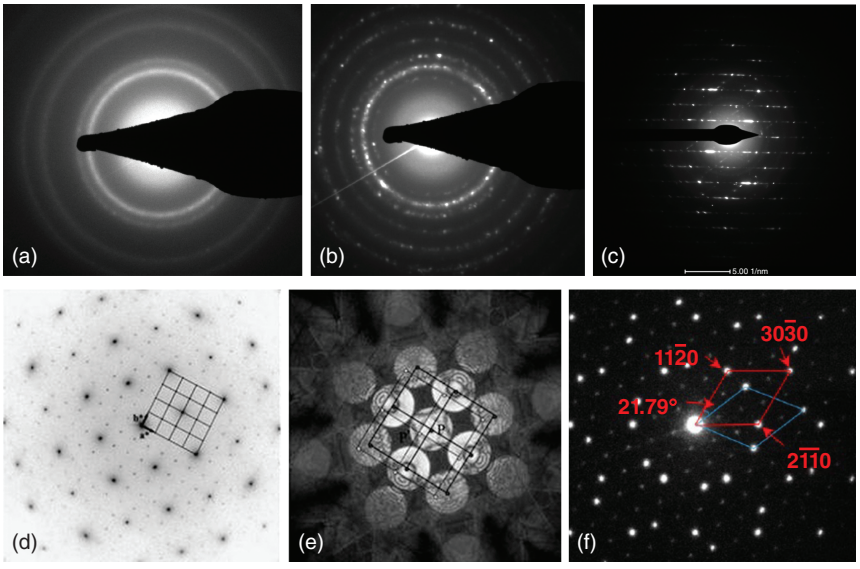

Figure 1.6 Selected area EDP with (a) continuous rings indicating amorphous nature of the sample, (b) rings with diffraction spots from polycrystalline sample, (c) streaks in ordered 2D pattern indicate presence of defects, (d) from single crystal Si oriented in [111] zone axis, (e) EBED from single crystal, (f) NED from a bicrystal α-Fe_2O_3, which can be indexed as two overlaying α-Fe_2O_3 platelets oriented along the $\langle 0001 \rangle$ zone axis, with a coincidence-site-lattice boundary with a twist angle of 21.79. Source: (d, e) Zhu et al. [16]/ from American Chemical Society.

electron diffraction by using parallel electron beam of nanometer size to select an area of interest and are known as NAEDs [21]. Nano-diffraction techniques allow as to meet the challenges of obtaining structural information from the building block of the nanoworld (Figure 1.6f). For example, chirality of individual single-walled nanotubes can be determined using NAED [22].

1.5.2 TEM Imaging Modes

The dual nature of electrons, as particles and waves, is used in understanding the image formation process. While the electrons scattered by the atoms or crystalline lattice propagate as transmitted electrons, the wave function makes the image formation similar to an optical microscope and fundamental mechanism also has some similarities. For example, the resolution can be defined by the Rayleigh criteria; separation between two-point objects should be more than 0.61λ, where λ is the wavelength of incident light. It implies that the image resolution can be improved by decreasing the wavelength, i.e. by increasing energy of the electrons. However, unlike light, electron scattering is both elastic and inelastic, and the Rayleigh's criteria do not hold as the resolution is impeded due to multiple scattering experienced by electrons while traveling through the sample and the magnetic lenses.

> The wavelength of the electron in such a microscope is only 1/20 of an angstrom. So it should be possible to see the individual atoms. What good would it be to see individual atoms distinctly?
>
> – Richard Feynman

In the high-resolution TEM, a parallel incident electron beam interacts strongly with the sample, forming multiple diffracted beams (as explained above) that are brought together by the objective lens such as they can interfere to create an image, and the structural information can be obtained from the exit electron wave function that has been attenuated by the multiple scattering events. We should keep in mind that the exit-wave carry the information about both the phase shifts and amplitude modification due to electron scattering by the sample. The phase information cannot be directly visualized as it is influenced by the lens aberrations and other imperfections; therefore, it is the amplitude of the electron wave that is recorded on the image plane.

However, we need the phase information of the exit waves to obtain structural information, which can be achieved by tuning the focus of the objective lens such that the phase of the wave is converted into amplitudes on the image plane. The combined effect of aberrations, objective aperture function, drift, and other instabilities on the image contrast can be mathematically treated as phase-contrast transfer function (CTF). Scherzer has shown that there is a specific value of defocus, depending on the properties of the microscope, where low spatial frequencies are transformed into image intensities with similar phase. This value, known as Scherzer defocus, also determines the resolution limit of the microscope. However, we should keep in mind that the information beyond Scherzer resolution can be obtained by using a highly coherent and monochromated electron beam generated by a FEG along with aberration correctors. Moreover, the phase difference can also be measured from interference patterns such as formed by using holography, where separate phase and amplitudes image are collected (Section 1.6.2).

As mentioned above, the location of the sample within the objective pole piece is critical for obtaining the best electron optical performance of the TEM. With appropriate choice of the microscope, imaging conditions, and modifications, TEM can be used to obtain morphological, structural, and chemical information. Some of them are described below as they are the ones that we utilize to follow dynamic changes during in-situ observations.

- **Low-magnification TEM:** is used to obtain morphological information such as size and shape of nanoparticles, particle size distribution, dislocations, measuring Burger's vectors.
- **High-resolution imaging:** atomic-scale information, including, but not limited to, from defects, grain boundaries, nanoparticles, etc.
- **Dark-field imaging:** objective aperture can be used to select the diffraction spots to form image that shows the corresponding region as bright, similar to STEM-ADF images.

- **Tomography:** 3-D images reconstructed from a series of images recorded at incremental positive and negative tilts (±70°). Full rotation of sample is possible by using needle-shaped sample geometry and a special TEM holder.

1.5.3 STEM

Image formation in a STEM is achieved by scanning a small electron probe across a thin sample. It is similar to SEM, except while secondary and/or back-scattered electrons are used for image formation in an SEM, forward scattered or transmitted electrons form a STEM image. On the other hand, reciprocity relationship can be found between TEM and STEM, where electron source and detector exchange their location while other components are the same. Also, while a parallel electron beam is used to form a TEM image, STEM image is formed by scanning focused electron probe, such that the STEM image resolution depends on the size of the electron probe. Integration with FEG source provides small probe size (0.1 nm or better in modern instruments) with enough intensity for imaging and chemical analysis. STEM has following advantages over TEM:

I. Electrons scattered at different angles contribute to formation of bright-field (BF), annular dark-field (ADF), or high-angle annular dark-field (HAADF) images and can be collected by using different detectors.
II. We can use the small probe to obtain atomic-scale chemical information using either EELS or EDS (chemical mapping).
III. Probe can be focused anywhere along the thickness (z-direction) of the sample, thereby providing a possibility to obtain 3-D information.
IV. HAADF images are sensitive to the atomic number (Z) of the atoms and are used to obtain chemical information directly from the intensity distribution in the atomic-resolution images.

Although there are dedicated STEM instruments still available, most of the modern microscopes can operate in both TEM and STEM modes. However, STEM is not generally used for in-situ dynamic characterization as the time resolution for acquiring images is longer than that for TEM imaging.

1.5.4 Analytical TEM

The strength of TEM/STEM is not only that we can obtain high-resolution images with 0.05–0.1 nm image resolution, with one-to-one correspondence between structure and the image, but also in the fact that we can obtain chemical information with spatial resolution of 0.1 nm to 10 nm. Spatial resolution of a TEM for obtaining chemical information depends on the probe formation characteristics of the TEM, i.e. the probe (spot) size and the current in the probe. As mentioned earlier, modern TEM has possibility to form a probe as small as 0.1 nm with enough beam current (0.2–0.3 pA) to generate enough EELS and/or X-ray signal to be collected in reasonable time (2 to 30 seconds time frame).

As explained above and shown in Figure 1.2, when a fast incident electron traverses through a thin sample, it may experience an inelastic scattering event in which energy and momentum from the incident electron are transferred to electrons

in the solid that will result in an electronic excitation event. During this process, electrons in the solid undergo transitions to vacant states above the Fermi level, and the atoms of the solid are ionized. The energy lost by the incident electron, ΔE, is then equal to the difference in energy between the initial and final states of the electron(s) being excited in the solid. A collective interaction of both inner- and outer-shell electrons may be involved in this excitation process. It is this fundamental interaction that gives rise to the EELS and the EDS signal and is used for chemical analysis.

1.5.4.1 Chemical Analysis

EDS The vacancy created in one of the inner-shell levels of an atom during the ionization process by fast-moving electrons may subsequently be filled by an electron moving down from an upper shell, and the energy difference is emitted as X-rays. The X-rays are labeled according to the initial and final states of the electron making the transition to fill the vacancy. For example, a vacancy in the K or L shell gives rise to the production of K- or L- X-rays. Greek letters are used to identify the initial state of the electron making the transition. For example, L to K transitions give rise to K_α X-rays, and M to K transitions give rise to K_β X-rays. The K_β X-rays are always of higher energy than the K_α X-rays. X-rays produced through these processes are characteristic of the element involved and are always emitted isotopically. With the help of suitable detector, EDS is used for chemical analysis of the sample. An example of EDS data collected from CdTe lamella in STEM mode is shown in Figure 1.7.

In addition to these characteristics X-rays, non-characteristic X-rays are also generated by the fast electron through a process known as Bremsstrahlung. Classically, this process can be considered in terms of a fast electron being slowed down by the field of the atoms in the sample. Here, it is this change in electron velocity that gives rise to X-ray emission. Bremsstrahlung gives a continuous background in the X-ray spectrum and must be removed to quantify the characteristic X-ray emission. The energy of the X-ray produced is directly related to the element present in the sample and the orbital level involved in the ionization process.

It is important to note that EDS detectors are sensitive to heat (due to infrared radiation) and gaseous environment and therefore not suitable for in-situ measurements

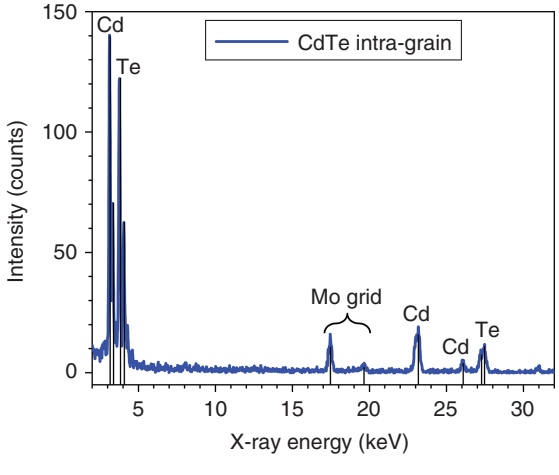

Figure 1.7 EDS from a CdTe solar cell lamella, collected in STEM mode, peaks from the TEM grid material (Mo in this case) are commonly present in the spectra. Courtesy: Wei-Chang (David) Yang, NIST.

under these conditions. However, the MEMS-based heating and gas cell holders have addressed this limitation [23, 24], although they have other problems as will be discussed in Chapters 3 and 7 in detail. Alternatively, chemical changes from the same area can be observed before and after reaction to directly correlate the effect of heat or environment.

Quantitative X-ray Analysis The EDS data are quite easy to collect and interpret and are often used for quantitative analysis. The first step in quantifying thin-film EDS data involves removal of the background to leave only the characteristic peaks of interest. The intensity of the remaining X-ray peaks can be expressed in terms of the atomic concentration, X-ray production factors, and instrumental parameters. For a thin film, the intensity of a characteristic X-ray from element A, I_A can be written as

$$I_A \propto I n_A \sigma_A \omega_A \varepsilon \tag{1.2}$$

where I is the total number of incident electrons, n_A is the number of atoms of element A per unit area, σ_A is the ionization cross section for producing a vacancy, ω is the florescence yield, and ε is the detector efficiency. For many applications, the quantity of interest is the relative concentration of one element with respect to another. The relative concentration of two elements then can be obtained using following equation:

$$C_{AB} = k_{AB} \frac{I_A}{I_B} \tag{1.3}$$

where we have combined all the terms involving X-ray generation and the detector efficiency into the quantity k_{AB}. This simple form is known as the Cliff–Lorimer equation for thin film X-ray analysis. It can be used to quantify X-ray spectra obtained from thin film provided that:

i. The electrons lose only a small fraction of their energy in the film and backscattering can be ignored.
ii. The specimen detector geometry is such that effects due to X-ray absorption and fluorescence can be ignored.
iii. Coherent scattering effects, which occur within crystals (such as channeling), have not been included in the derivation of the above two expressions. Whenever possible, crystals should be tilted away from strong diffracting conditions to avoid systematic errors in the analysis.

For a fixed accelerating voltage and detector geometry, the k-factor for each pair of elements is constant. The simplest way to determine the k-factor for a given microscope is to measure them directly using standards of known composition. Numerous tabulations of k-factors are now also available in the literature. It is also possible to determine k-factors using known values of the X-ray generation parameters for each element. In this case, it is also necessary to know the form of the efficiency function, ε, for the detector involved. It is generally assumed that the most accurate k-factors are obtained by measurements from standards. However, the standard-less approach can be useful when suitable standards are not available for the elements of interest.

EELS As explained above, during X-ray emission, an electron from one of the higher orbitals falls into the lower energy state to fill the vacancy. The energy lost by electrons during initial excitation to create the vacancy is also characteristic of the atom involved and allows elemental analysis to be performed. By adding a magnetic spectrometer beneath the viewing chamber, the energy distribution of electrons that have passed through a thin specimen in a TEM is measured (Figure 1.3) to obtain the EELS data. Another method, not very commonly available, is by using an in-column energy filter (Omega filter), located below the sample, to collect EELS data. The spectral energy resolution is largely determined by the energy span of the electron source: i.e. 1–2 eV for a thermionic source, 0.5–0.7 eV for FEG, and 0.01–0.1 eV for an FEG with a monochromator. Figure 1.8a shows various types of EELS peaks arising from interactions of electrons with atoms in the sample. Most of the high-energy electrons are transmitted through the sample with negligible loss of energy and constitute zero loss peak that has the highest intensity. Its full width at half maxima (FWHM) is the measure of energy resolution that is controlled by the source as well as by the spectrometer. Elastic scattering of the electrons by the nucleus gives rise to low-loss peaks such as plasmon peaks, and their number increases with the thickness of the sample. Low-loss region may also have peaks that can be attributed to vibrational and phonon modes, localized surface plasmon resonance, and bandgap of the material. Inelastic scattering results from the interaction with electron cloud around the sample, and the energy lost is generally higher than 50 eV (Figure 1.8a). Electron–electron interactions result in knocking out electrons from the outer or inner shell, and the energy as well as shape of these peaks is specific to the element as well as to the bonding environment (Figure 1.8b) (see Egerton's book [27] for more info). Since the electron beam can be focused into a probe of sub-nm dimensions

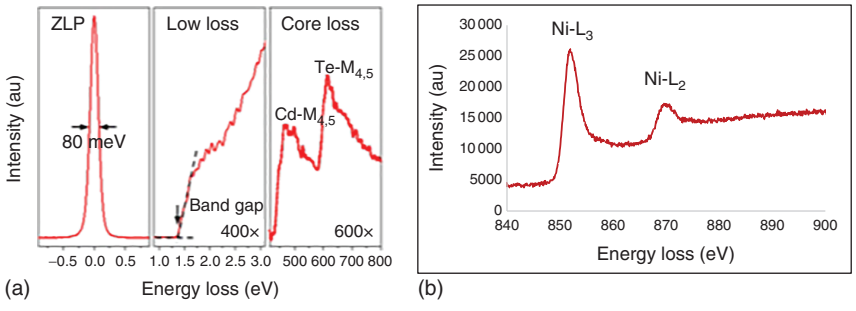

Figure 1.8 (a) Zero-loss, low-loss, and the core-loss regions of EEL spectra acquired in STEM mode from CdTe solar cell lamella using dual EELS detector. The intensities from low-loss and core-loss regions are magnified by 400× and 600×, respectively, for visualization purpose. FWHM of ZL peak is a measure of energy resolution of the source, low-loss region can be used measure the bandgap (shown here), plasmon, and LSPR energies (not shown here but check Figure 3.5 for plasmon energy applications). Courtesy: Wei-Chang (David) Yang, NIST. (b) Core-loss region showing Ni-L_2 and Ni-L_1 peaks, often termed as white lines. For most of the transition metals, white-line ratio and the onset of core-loss peaks can be used to determine their oxidation state. Source: Adapted from Refs. [25, 26].

at the specimen, this spectral information can be obtained with very good spatial resolution [6, 28]. We can use the EELS to obtain following information:

Thickness of the Sample The energy-loss spectrum can be employed to measure local specimen thickness. This relies on the fact that for incoherent scattering, the relative intensity of the zero-loss peak decreases monotonically with increasing thickness. The sample thickness t can be written as

$$t = \lambda L_{\mathrm{n}}(I_{\mathrm{tot}}/I_{\mathrm{o}}) \tag{1.4}$$

where I_{tot} is the total integrated spectral intensity, I_{o} intensity of the zero-loss peak, and λ is a parameter called the inelastic mean-free path. This equation is quite simple to use and can be used to measure sample thickness between 5 and 500 nm.

Qualitative Elemental Analysis The inner-shell excitations show up as ionization edges, and their onset position corresponds to the ionization potential of the electron involved in the Coulomb interaction between the incident electrons and atomic electrons. For thin samples, most of the electrons do not lose energy, and zero-loss peak is much stronger than inner-shell excitation edges. Therefore, it is easy to identify edges from thin samples. EELS is very effective to identify light elements such as carbon, oxygen, and nitrogen.

Quantitative Elemental Analysis Quantitative analysis using EELS is not as straightforward as for EDS analysis and generally should be used only if the same information cannot be obtained from the EDS data. The intensity distributed on $I_{\mathrm{A}}(E)$ in an inner-shell edge from element A in a thin film can be written as

$$I_{\mathrm{A}}(E) = IN_{\mathrm{A}}\frac{\mathrm{d}\sigma_{\mathrm{A}}}{\mathrm{d}E} \tag{1.5}$$

where I is the number of incident electrons, and N_{A} is the number of atoms of type A per unit area. The quantity $\mathrm{d}\sigma_{\mathrm{A}}/\mathrm{d}E$ is known as the energy-differential cross section (See Egerton's book for more info [27]), which is difficult to quantify, therefore making quantitative analysis challenging.

Bonding Information The onset energy, shape, and number of peaks in core-loss spectra are fingerprints of electron densities in the valence band. Therefore, depending upon the spectral resolution of the microscope, they contain the information about the bonding with the first, second, and other nearest-neighbor atoms. Careful examination of ionization edges reveals the band structure as oscillations within the first 20 or 30 eV of the edge onset, which are referred as near-edge structures. A comparison between theoretical model and experimental spectra can be used to obtain bonding information of the element.

Detailed interpretation of near-edge structure remains a topic of ongoing research, but some general applications are outlined below:

- Changes in the shape of ionization edge structure signify a change in the chemical environment around a particular element, i.e. bonding.

- For 3d and 4d transition metals, the intensity of the peaks at the threshold (the so-called white lines, Figures 1.8b and 4.14) can be correlated with the number of vacant states in the d bands of the materials, i.e. valence state.
- Temperature measurement using plasmon peak shift [29].
- Pressure measurement from plasmon peak shift [30].

We can use EELS to fingerprint different chemical environments for identification of compounds. EELS is routinely used for in-situ monitoring of chemical state of the sample as function of temperature and environment (liquid or gas) as explained in Chapters 3,4, 6, and 7.

1.5.4.2 EFTEM

EELS spectrometer can also be used to obtain images or DPs using the electron within a selected energy window and filtering out the rest, generally known as EFTEM. There are two types of filters commercially available: (i) in column filter (Omega or Wein) and (ii) post projector filter (Gatan Imaging Filter, GIF). Each system has slits to choose the windows between 5 and 100 eV for image/DP formation. Zero-loss images/DPs are obtained by choosing between 5 and 15 eV window, centered at the zero-loss peak, i.e. using only elastically scattered electrons. This method is used to obtain high-contrast images from thick samples. DPs obtained from elastically scattered electrons are used for structure determination as the intensities can be directly used to obtain structure factors (for more information, see Zuo and Spence [5]).

Images obtained using specific ionization intensities are used to obtain a distribution of certain element within the image or an elemental map of the sample. In order to obtain quantitative information, the contribution from the background must be subtracted. This can be achieved by following two ways:

(a) **Three window maps:** For quantitative elemental mapping, we select two pre-edge energy windows to form pre-edge images and another window centered at the elemental peak to form post-edge image (Figure 1.9). If the two pre-edge energy windows are adjacent to each other, they can be used to evaluate the background parameters, A and r, and background is calculated assuming the background has a form AE^{-r}. The background contribution thus can be subtracted from the post-edge image to obtain the image that contains the contribution only from the ionization edge intensities, i.e. elemental map [27].

(b) **Jump ratio maps:** It is simple method to obtain an elemental map and is particularly useful when pre-edge section is not wide enough to select two windows for collecting pre-edge images, as one of them might be overlapping with ionization edge of another element. Jump ratio maps, as the name implies, are obtained by recording imaged from (i) one pre-edge window for background and (ii) one for the ionization edge window of a specific element. A new image is then generated by dividing post-edge image by pre-edge image. This method yields a jump ratio map that is insensitive to the specimen thickness and diffracting conditions [27]. Both methods are routinely used.

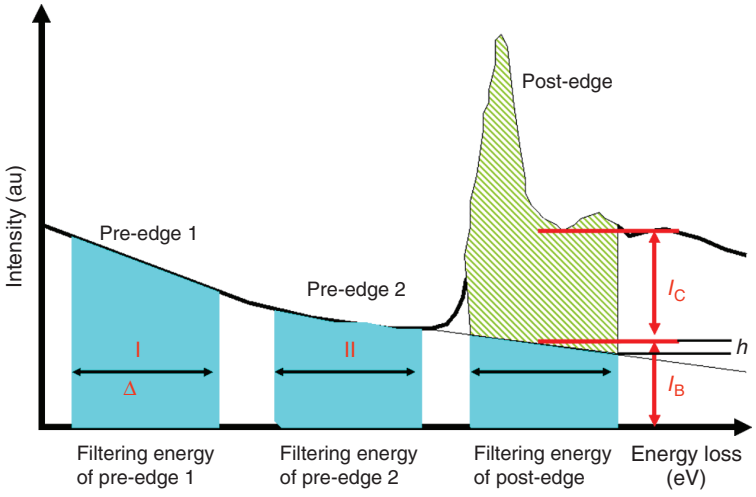

Figure 1.9 Schematic showing the process of choosing windows for collecting filtered images from two pre-edge and the ionization windows used to obtain an elemental map. The number of counts in background and edge spectra are marked as I_g and I_c, respectively. For jump ratio map, images from one background and ionization edge window are collected. Source: Egerton et al. [27]/Springer Nature.

1.5.4.3 Spectrum Imaging (SI)

Spectrum imaging (SI) is another method to use analytical data to obtain elemental maps. It is performed in STEM mode to collect either EDS or EELS signal from each pixel of the image. These scans provide 3-D data sets that are then used to obtain elemental distribution map at atomic scale [5, 31, 32]. Just as for the STEM imaging, the spatial resolution for SI is defined by the probe size; therefore, atomic-resolution elemental maps can be obtained using a monochromatic electron beam combined with C_s-corrected probe forming lens. The resultant image is like a normal TEM image, except each image pixel contains entire EELS or EDS data. Thus, the 3-D data cube (Figure 1.10) obtained can then be sliced to get 2-D information in any direction and allows us to perform quantitative and statistical analysis.

> God runs electromagnetics on Monday, Wednesday, and Friday by the wave theory, and the devil runs it by quantum theory on Tuesday, Thursday, and Saturday
>
> – Sir Lawrence Brag

1.6 Other Techniques

1.6.1 Lorentz Microscopy

Behavior of magnetic materials, just like others, is controlled by their nanoscale structure. Therefore, we need to determine a structure–property relationship, both for understanding fundamental science as well as for their potential applications in magnetic logic and memory devices. Lorentz TEM is ideally suited to find structure

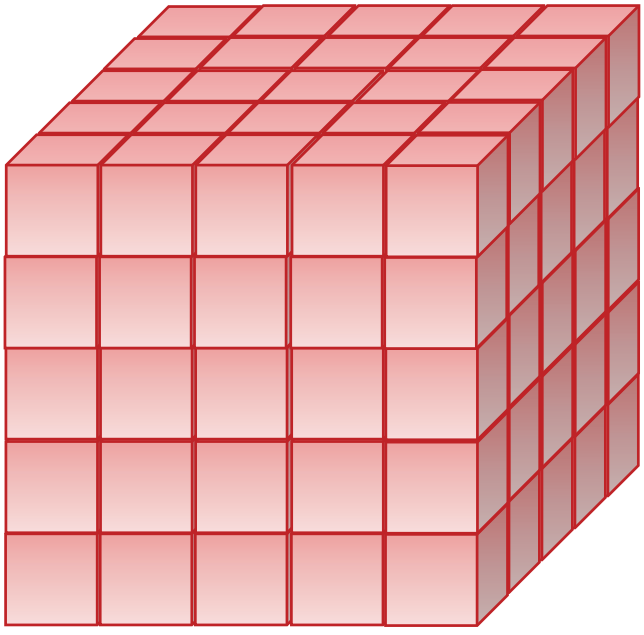

Figure 1.10 Schematic of a "data cube" obtained by collecting EELS data from each pixel in STEM mode. An elemental map can be produced using EELS spectrum thus collected.

and magnetic property relationship by determining the crystal and magnetic domain structures in correlation with their physical properties. For magnetic materials, the electron beam is deflected due to Lorentz interaction, arising from in-plane magnetic induction perpendicular to the electron beam. Therefore, the part of the sample, magnetized in-plane, can be imaged easily, and the part with perpendicular magnetization will need to be tilted to produce the same amount of deflection. The angular deflection, known as β, is given by $\beta = e\lambda B_s t/h$, where B_s is saturation induction, t is thickness of the sample, e is the magnitude of the electronic charge, λ is the wavelength of the electrons, and h is Planck's constant. We find that Lorentz microscopy can be used for both the qualitative and quantitative measures of the magnetic behavior of thin films [33, 34].

However, we must realize that in a TEM, the sample is immersed in high magnetic field of the objective lens that can alter or destroy the magnetic structure entirely. Therefore, we need a TEM with modified objective lens that can be switching off and use projector lenses for imaging. Other strategies such as adding a shielding around the objective lens to reduce the field or changing the pole pieces, etc. are also available [35].

Again, in the last few decades, we have moved from static imaging to in-situ investigation of effect of magnetic-field or temperature on the nanoscale configuration of magnetic components such vortices, skyrmions, bubbles, and phase transformation related to ferro- and ferrimagnetic properties [36, 37]. It is a developing field of research, and multiple imaging techniques such as Fresnel and Foucault modes, electron holography, and differential phase contrast (DPC) techniques are being applied [38, 39]. In-situ manipulation of magnetic domains, topological features,

vortices, and skyrmions, using electrical current, magnetic fields, and temperature, has revealed novel phenomena that advance the development of nanodomain-based devices and spintronics [40–45].

1.6.2 Holography

As explained in Section 1.5, the exit wave from the sample varies in intensity due to electron–sample interaction and contains both the phase and amplitude information. The contrast in the TEM images represents the amplitude modulation of the exit wave, and phase shifts, although present, cannot be directly visualized. We need to find an alternate method to obtain phase images along with an amplitude image. However, retrieval of phase information is not simple as it is attenuated by the lens aberration, aperture function, etc. but can be deconvoluted using holography [46]. Cowley has identified 20 forms of electron holography [47], including in-line and off-axis holography that are briefly described below.

1.6.2.1 In-Line Holography

Two methods, Fresnel images and reconstruction of focal series, constitute in-line holography. Fresnel images are used to recover phases by minimizing the error function between simulated and experimental image intensities [48]. Image reconstruction from focal series to retrieve phase information is used to obtain 3-D shape of nanoparticles without the need to tilt the sample, unlike electron tomography [49]. The possibility to record atomic-resolution images using the aberration-corrected microscope extends our ability to obtain 3-D atomic-scale information by applying phase reconstruction algorithms to a focal series [46]. Another advantage of this method is that the dose rate for recording individual image can be adjusted to mitigate the electron-induced damage to the sample, i.e. image series can be acquired under low-dose conditions [50]. However, in-line holography requires tedious algorithms and computer time.

1.6.2.2 Off-Axis Holography

D. Gabor (1949) presented the idea to recover phase from electron microscope images using interreference methods such that the information lost by the lens imperfections can be restored [51]. However, it could not be fully developed due to the incoherent electron sources used at that time. After the advent of FEG electron source becoming commercially available, and development of electrostatic biprism, two crucial requirements for off-axis electron holography, the technique has been further developed [52–55]. Briefly, the method constitutes obtaining an image, after applying positive voltage to the biprism, where exit wave from the object superimposes an unscattered (reference) wave passing through the vacuum at an angle. The phase shift experienced by the electrons traveling through the sample can be retrieved from the image that is a direct measure of electrostatic potential and in-plane magnetic component in the sample. Therefore, off-axis holography, in combination with Lorentz microscopy, is frequently employed to study the strain in the sample and the magnetic properties of the materials [56–59].

1.6.3 UEM and DTEM

The main motivation behind time-resolved in-situ TEM observations is to reveal intermediate steps and/or transient phases that lead to the final product. Whereas TEM-based imaging, diffraction, and spectroscopy techniques are ideally suited to obtain 2D and/or 3D information at high spatial resolution, the time (temporal) resolution (fourth dimension) is limited to the acquisition rate of the recording media, currently reaching 1 ms by using a direct electron camera (e.g. Gatan's K3). Another way to overcome this limit is to reduce the electron emission time interval, used for recording diffraction, images, or chemical composition, such that recording media time becomes obsolete. Thus, we can uncover intermediate steps of the processes and visualize transient states, such as diffusion less phase transformation, dislocation motion, nucleation events, etc. that occur at a lightning speed. In past couple of decades, pump-probe approach has resulted in the development of ultrafast electron microscopes (UEM) and dynamic transmission electron microscope (DTEM) that has improved the time resolution to the order of femto seconds [60–64].

An UEM, first developed in Ziweil's group at California Institute of Technology, the thermionic source for electron, is replaced by a photo electron emission from a cathode (Figure 1.11a). The electron emission is achieved by using femtosecond laser pulses, a stroboscopic approach that generates single or few electron packets, used for imaging, diffraction, or spectroscopy. The temporal resolution is limited

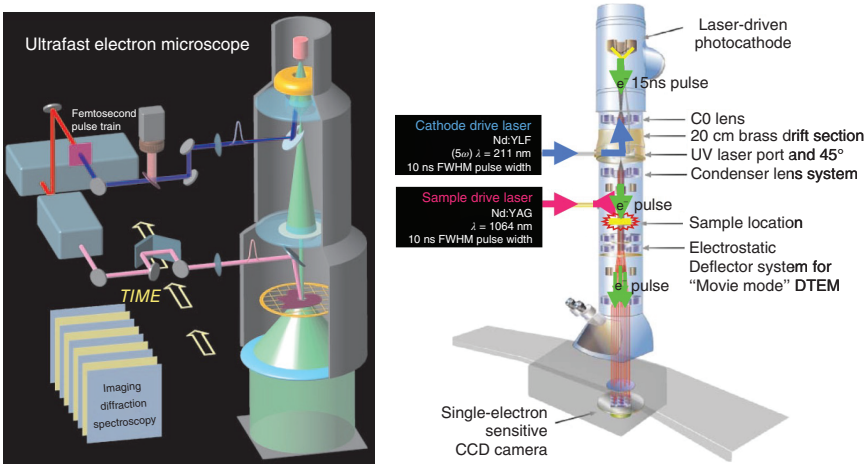

Figure 1.11 (a) The ultrafast electron microscope. Shown are the basic components, which involve interfacing the TEM with a train of femtosecond optical pulses to generate the on-axis electron beam in ultrafast packets of about one electron per pulse. The other optical beam delivers, after a well-defined delay time, initiating pulses at the specimen, thus defining the zero of time. Source: Lobastov et al. [65]/National Academy of Science. (b) Schematic of the DTEM from Lawrence Livermore National Laboratory (LLNL showing the modifications needed to convert a TEM into DTEM. Note that both technologies are based on the basic principle of pump probe but differ in the electron pulse rate and design philosophy. Source: LaGrange et al. [66]/With permission of Elsevier.

by the laser pulse rates used for electron emission, but the spatial resolution is compromised due to low signal-to-noise ratio. An improvement in spatial resolution is achievable only by recording a reversible phenomenon multiple times and averaging the images to obtain SNR with enough contrast to distinguish specific features. However, we need more electrons in a single shot to observe irreversible processes that is achieved using "pump-probe" method in a DTEM (Figure 1.11b). Here, the sample is subjected external stimuli (pump), and the effect is recorded (probe) with a suitable time interval [67]. Currently, two separate lasers are used, one as an external stimulus to bring the sample to a transient state and the other to generate photo electrons. As is obvious, the technology requires major modification to the conventional TEM column [68]. Recently, DOE and NIST team has eliminated laser excitation for electron pulse generation by placing RF cavity combs as tunable electron pulser between electron source and condenser lenses and have achieved picosecond resolution by generating electron pulses at GHz rate [69, 70]. These are developing techniques, and the TEM is modified in-house by the researchers, which has limited their applications to a small group of researchers.

1.7 Introduction to Different Stimuli Used for In-Situ TEM

During last few decades, a large number of TEM holders, as well as dedicated TEM for a specific application, have been developed to follow nanoscale changes in a material under different stimuli. In this book, we will explain the development, functioning, and applications of following stimuli:

1.7.1 Heating (Chapter 3)

Effect of thermal stimuli in vacuum, to decipher phase change, nucleation, dislocation formation and motion, decomposition behavior, etc.

1.7.2 Cooling (Cryo TEM – Chapter 4)

Low-temperature behavior of materials is obtained using time- and temperature-resolved imaging, diffraction, and spectroscopy, especially for magnetic phase transition, ice formation, glass transition, nucleation and precipitation, and other reactions in liquids using plunge-freeze technology, etc.

1.7.3 Interactions with Liquid/Electrochemistry (Chapter 6)

It is a growing field of research as it impacts several real-world problems such as corrosion, functioning of battery materials, and water splitting to produce hydrogen and oxygen.

1.7.4 Interaction with Gas Environment/Catalysis (Chapter 7)

This is another growing field with similar impact with applications including catalysis, redox processes, and corrosion.

1.7.5 Other Stimuli Not Included in this Book

1.7.5.1 Mechanical Testing

Applications of metals, alloys, and ceramics are dependent on their mechanical properties (plasticity and elasticity) that in turn are controlled by the atomic structure, grain size, grain boundaries, and defects, such as dislocations. Therefore, understanding the structure–property relationship is important for defining their scope and generating practical guidelines for their applications. We expect that understanding fundamental principles that define the structure–property relationship will result in designing materials with improved properties. Generally, the structure–property relationship is established by making static measurements, e.g. by finding the fracture point of a material and imaging it before and after the load (stress or strain) was applied. However, we cannot establish the structural changes that lead to the fracture by static characterization and dynamic in-situ measurements are needed [71].

> Breaking something is easy…understanding how it breaks is a different story
>
> – Andrew Minor, UC Berkeley

In past couple of decades, nano-indenters have been developed by individual research groups as well as by commercial companies [72–75]. Basic design of a nano-indenter is shown in Figure 1.12, where a pyramid-shaped diamond intender with a tip diameter of about 100 nm is attached to a shaft with a micrometer and piezo-drive capable of moving the intender tip in all three (x, y, and z) directions. The micrometer is used for rough alignments of the intender tip on to the sample, while piezo drive is used for fine-tuning and applying force on the sample. These advances in the design and functioning of nano-intender TEM holders, along with easy access to aberration corrected TEM, have made it possible to observe and measure the nucleation and motion of dislocations as a function of loading [76–79]. Here the sample preparation is also crucial for making successful measurements as the sample must be electron transparent, accessible to the intender tip, and mechanically stable such that force applied effects only the region of interest and does not bend the entire sample. The applications include, but are not limited to, measurement of elasticity/plasticity, nucleation and motion of dislocations, nucleation and annihilation of grain boundaries, etc. [59, 65, 66, 80, 81].

1.7.5.2 Ion Radiation/Implantation

Ion radiation damage to materials, such as metals, alloys, and ceramics, in specific environments alters their properties and applicability. Understanding

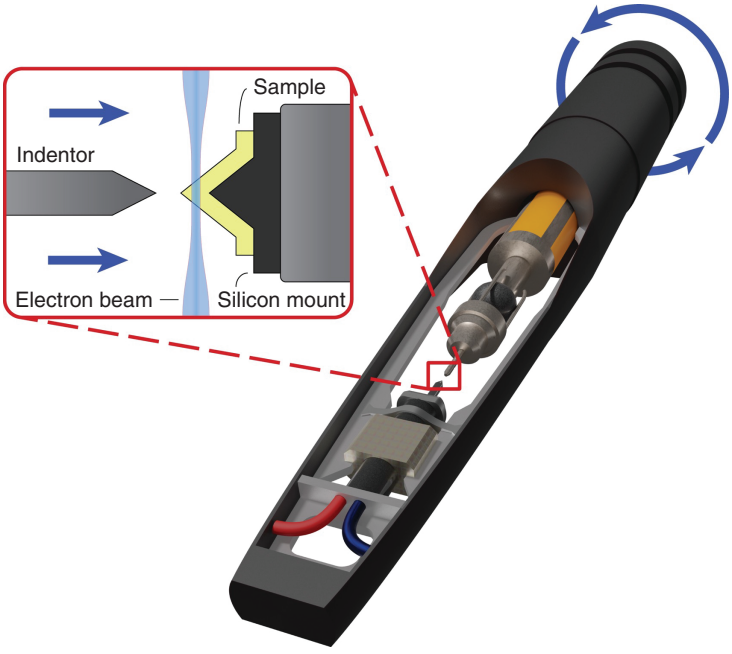

Figure 1.12 Schematic showing the tip of a nano-indenter holder with magnified region from the red square showing the sample mount and indenter location. Blue region represents the electron beam.

the phenomenon is especially crucial for the materials to be used in space and nuclear plants. Controlled irradiation, coupled with TEM, can be used to simulate the structural transformations caused by α- and/or β-decay, neutron, or fission fragments. As new nuclear reactor technologies are being developed, damage to the materials used over time has become more and more important. Intentional ion radiation is an expedited way to understand and measure the damage that may take years to happen in real reactor environment. Here, in-situ TEM observations provide unprecedented atomic-scale knowledge about the segregation within the material, formation of precipitates, defects and/or dislocations, etc. under the ion beam radiation [82, 83]. There are two main advantages of this exercise: (i) the life expectancy of a reactor material can be evaluated in short period by increasing the radiation dose to the levels expected for a longer period in the reactor, and (ii) a priori knowledge can be used to design new materials with improved properties.

Although small ion guns have been directly mounted on the TEM column, most of the facilities utilize free-standing ion accelerators. As expected, incorporation of an ion beam source in the TEM column is neither simple nor easy as ion accelerators are quite bulky and TEM column must be modified for ion beam to access the sample. Figure 1.13 shows layout of a dual-beam (medium and low energy) ion accelerator and its connectivity to the TEM, installed at University of Huddersfield, UK [84]. This system, named as MIAMI-2, occupies a two-story building, specifically built to house it. Similar systems, with up to triple-beam accelerators, are also available at few other places in the world, such as Xiamen

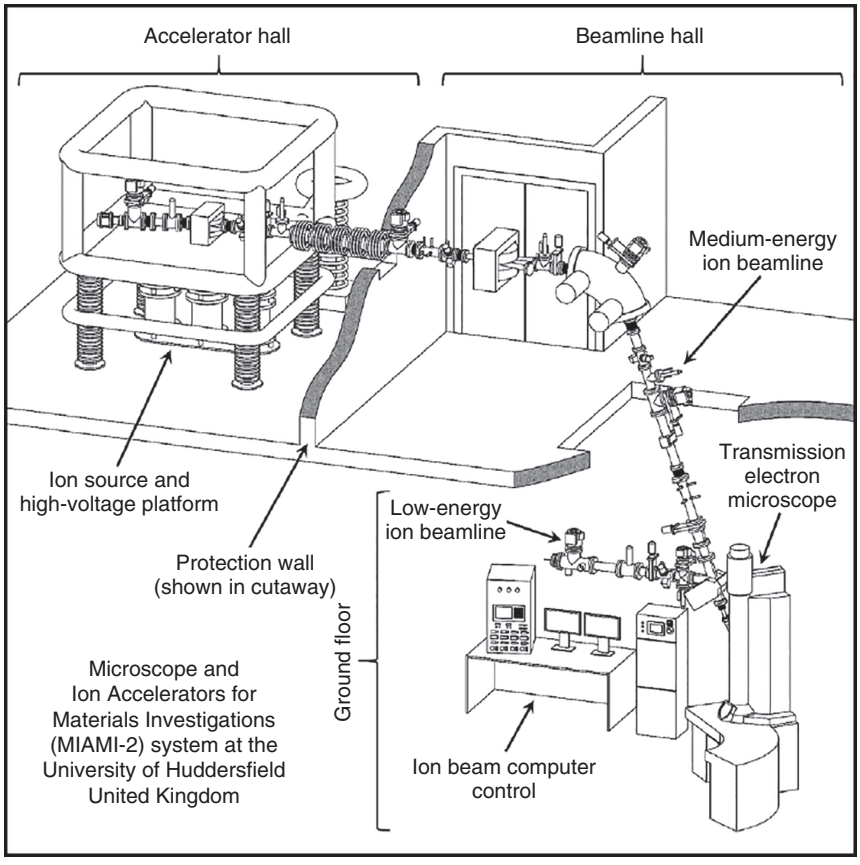

Figure 1.13 Overview of the layout of the MIAMI-2 system, which incorporates two ion beams that can be combined before entering the microscope. Source: Greaves et al. [84]/Elsevier/CC BY-4.0.

University, China [85]; Orsay, France [86]; University of Michigan, USA [87]; Sandia National Laboratory, USA [88], to name a few.

Lian et al. have combined a host of TEM-based techniques, such as TEM and *Z*-contrast imaging, EELS, and EFTEM, to decipher the effect of ion and electron radiation on complex ceramic materials [89]. Other similar studies include, but are not limited to, investigating the effect of ion radiation on ferric materials [90], formation of dislocation loop [91], nanoparticles of oxide dispersion strengthened (ODS) steels and austenitic steel [86], boron carbide [86], amorphization of an equiatomic martensitic NiTi alloys [92], effect of ion-radiation-induced amorphization of ABO_3 compounds on recrystallization [93], synthesis of nanosized bicrystalline (Pb, Cd) inclusions in Al by sequential ion implantation [94].

1.7.5.3 Biasing

Biasing the sample with known variable electric current is used to (i) generate magnetic/electric fields in the sample [95–97], (ii) trigger electromigration in sample [98], (iii) measure the *I*–*V* relationship [99], and (iv) conductance measurement

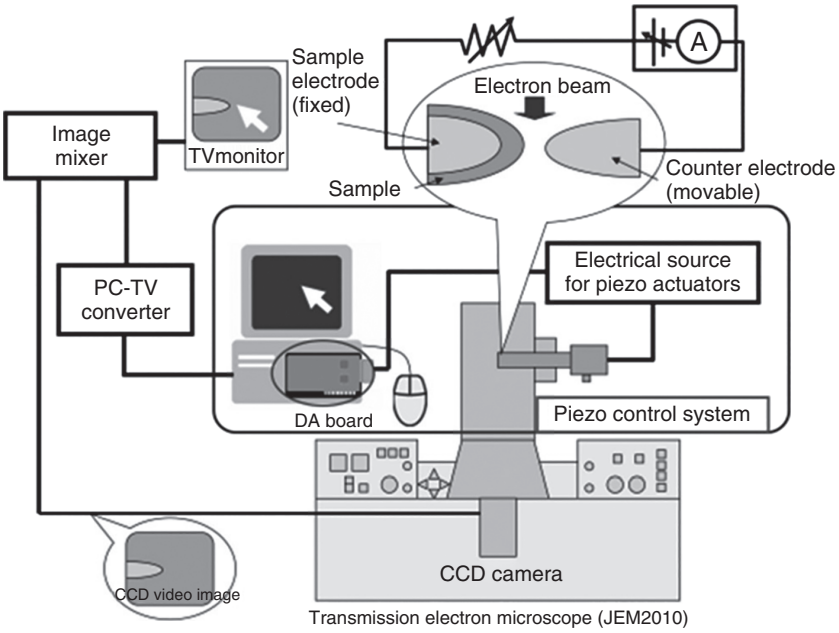

Figure 1.14 A schematic showing the entire system used for *I*–*V* measurements, where the modified holder with specimen and counter electrode (magnified image shown in balloon) that is aligned with respect to the sample using a piezo control system. Images are recorded the CCD camera of TEM. Source: Fujii et al. [99]/AIP Publishing LLC.

of nanostructures [100, 101], that reveal the structural modifications of electrode materials under operating conditions [102, 103]. In-situ TEM observations and measurements are performed using modified holders that are commercially available. Both the sample geometry and holder modifications depend on the type of measurements to be performed. For example, *I*–*V* curve measurements are done by scanning a flat surface, nanowire, or nanotube using an AFM/STM tip incorporated in the modified holder [102, 104]. A schematic of experimental plan used by Fujii et al. to make *I*–*V* measurements of NiO nanoregions is shown in Figure 1.14 [99]. They also developed a special holder with three main functions: First is to position the electrode with sub-nanometer accuracy with respect to the sample region; the second is to measure the current in nano-amp range using a built-in amplifier that can be switched off to measure larger currents; the third to measure the load using a semiconductor sensor [99]. By applying a voltage between the probe-tip and epitaxial bottom electrode, the TEM-STM holders can also be used to induce electric field along the film normal [105].

1.7.5.4 Magnetization

Magnetic nanostructures and thin films are of materials of interest due to their technological applications as random-access memory devices, magnetic recording media, ferroelectric field transistors, spintronics, etc. [38, 106]. The properties of these ever-shrinking structures are controlled by their morphology, shape, length, and distribution of magnetic domains within the nanostructure [43].

Nanoscale characterization of magnetic components within thin films and/or other nanostructures can be achieved using Lorentz microscopy [41, 106], or holography [107], or a combination of the two [108]. However, since their structure and properties change as a function of magnetic field and temperature, in-situ TEM observations and measurements are needed to establish a correlation between the structure and applied magnetic field or with temperature.

Controlled magnetic fields around the sample can be achieved in various ways such as by controlling the current in the objective lens [109, 110] or using a modified specimen holder [108, 111]. By exciting the standard objective lens to reduced levels, combined with sample tilt, it can be used manipulate the micromagnetic structure. This method allows us to design magnetization with other stimuli such as heating/cooling using appropriate holder or under different environments. However, the extent of magnetization by using this method is restricted by the inherent properties of the objective lens, and the perpendicular component of the objective can lead to distortions due to the sample geometry [112]. Alternatively, special magnetization holders have been built by incorporating a pair of electromagnets or coils [113]. Domain wall motion and switching [44, 109, 112], magnetization and demagnetization behavior [38, 114], hysteresis loops [109, 110, 115], formation and movement of vortices [111, 116], and skyrmions [117–119] are a few examples where in-situ TEM has played a crucial role in deciphering the magnetic behavior of nanostructures.

1.8 Potential Limitations and Cautions

As described above, last two decades have seen an unprecedented growth in the application of various in-situ techniques to explore and unveil atomic-level mechanisms involved in synthesis and functioning of nanomaterials, establish structure and property relationship, due to unprecedented developments in instrumentation and techniques. However, the more we have learnt about the applications, the more we have realized that the just like any other method, in-situ and operando measurements have their limitations. Some of the prominent ones, currently faced, are given below, whereas specific for different stimuli are explained in relevant chapters.

- **Reaction conditions:** Thermodynamic conditions, temperature, and gas pressure, achievable for in-situ TEM observations, are limited due to the instrumentation constraint. Similar restrictions are also applicable for other stimuli, such mechanical stress or electrical biasing.
- **Reaction time (not too fast nor too slow):** For us to observe and measure changes in the structure, chemistry, or property as a result of an external stimuli is very much dependent on the kinetics of the reaction. Therefore, we need a recording media that matches the reaction rate; otherwise, we will miss intermediate steps that may be important in controlling reaction. Gatan's K3 and other direct electron cameras have capability of image acquisition rate in the ms range, but the contrast in the images is very poor. However, we can obtain images with reasonable contrast with a time resolution of 0.025 seconds by averaging drift-corrected images acquired at higher rate.

Both EELS and DP can be acquired with higher temporal resolution and may be used instead of imaging if possible. UTEM and DTEM are other two techniques in development stages and currently limited to heating only.

What if the reaction is too slow? It is not practical to occupy the TEM for days to follow a reaction and may not be possible to monitor unless we can find a way to expedite it.

- **Reaction kinetics:** It is very tempting to measure the reaction rates and derive activation energies at nanoscale and compare them with theoretical or other experimental values. However, it can be elusive as the exact temperature of the observed area is questionable. The temperature measurement is further discussed in Chapters 3 and kinetics measurements in 2.
- Surface effects may dominate the process such that reaction mechanism of thin samples is not representative of bulk process. We can use STEM and/or tomography for 3D information at the cost of temporal resolution. We can also use bulk characterization techniques, such as X-ray diffraction to validate the TEM results (see Chapter 8).
- Last but not the least, limitation is due to ever-present electron beam effects. We should keep in mind that the images, DPs, spectroscopy data are all generated due to the interaction of high -energy electrons with the sample. Also, electrons interact with environment and ionize gas or liquid molecules, all of which can have negative consequences, especially making it difficult to distinguish between the electron beam affect and external stimuli.

> The rule of thumb is that electrons are affecting your sample unless proven otherwise
>
> – Peter Crozier, Arizona State University

However, all is not lost, as we can easily observe and even quantify the effect electron irradiation by (i) imaging the same area with "beam on" and "beam off" conditions, (ii) quickly moving to a previously unirradiated part to check if reaction starts again, and/or imaging unirradiated regions of the sample after external stimuli have been removed, i.e. the sample is cooled down. As we will see in Chapters 3 and 6, we can employ the electron energy to initiate certain reactions, which may be to our advantage as multiple sets of observations can be made from the same sample under same condition by just moving the beam to new areas.

Also, we have the possibility to mitigate the electron beam affects by reducing (i) the operating voltage and/or (ii) the electron dose. We can perform experiments to systematically measure the conditions affecting the sample and find a condition where the beam effects are eliminated or minimized. Keep in mind that this may not always be possible, and we may not be able to follow certain reactions using in-situ TEM techniques.

> The fact that we can "see" the electron-beam-induced changes makes it possible to determine the effect and find ways to mitigate it.

1.9 Take-Home Messages

- Motivation to make in-situ TEM/STEM observations arises from the shrinking of the technology world to nanosize.
- Most of the TEM-based techniques, combined with appropriate stimuli, can be used to decipher the morphological, structural, and chemical changes occurring during the synthesis and/or functioning of nanomaterials.
- Modification to either the TEM column or the specimen holders or both has enabled us to formulate structure–property relationships at nanoscale.
- The methodology has its limitations that should be considered.

References

Vendors Websites

Microscopes

1. Thermo Fischer: https://www.thermofisher.com/us/en/home/electron-microscopy/products/transmission-electron-microscopes.html
2. Hitachi: https://www.hitachi-hightech.com/global/science/products/microscopes/electron-microscope/tem
3. JEOL: https://www.jeolusa.com/PRODUCTS/Transmission-Electron-Microscopes-TEM
4. NION: http://www.nion.com/products.html

Specimen Holders

1. DENSsolutions: https://denssolutions.com
2. Gatan: https://www.gatan.com/products/tem-specimen-holders
3. Hummingbird: https://hummingbirdscientific.com
4. Protochips: https://www.protochips.com
5. Fischionne: https://www.fischione.com/products/holders
6. Mel-Build: https://melbuild.com

Articles

1 Knoll, M. and Ruska, E. (1932). Das Elektronenmikroskop. *Zeitschrift für Physik* 78: 318–339.

2 Williams, D.B. and Carter, C.B. (2009). *Transmission Electron Microscopy*, 2e, vol. 1–4. New York: Springer.

3 Muller, D.A. and Grazul, J. (2001). Optimizing the environment for sub-0.2 nm scanning transmission electron microscopy. *Journal of Electron Microscopy* 50 (3): 219–226.

4 Tiemeijer, P.C., Bischoff, M., Freitag, B., and Kisielowski, C. (2012). Using a monochromator to improve the resolution in TEM to below 0.5 Å. Part I: creating highly coherent monochromated illumination. *Ultramicroscopy* 114: 72–81.

5 Pennycook, S.J. and Colliex, C. (2012). Spectroscopic imaging in electron microscopy. *MRS Bulletin* 37 (1): 13–18.

6 Muller, D.A., Kourkoutis, L.F., Murfitt, M. et al. (2008). Atomic-scale chemical imaging of composition and bonding by aberration-corrected microscopy. *Science* 319 (5866): 1073–1076.

7 Rose, H.H. (1990). Electrostatic energy filter as monochromator of a highly coherent electron source. *Optik* 86: 95–98.

8 Krivanek, O.L., Ursin, J.P., Bacon, N.J. et al. (2009). High-energy-resolution monochromator for aberration-corrected scanning transmission electron microscopy/electron energy-loss spectroscopy. *Philosophical Transactions of the Royal Society A: Mathematical, Physical and Engineering Sciences* 367 (1903): 3683–3697.

9 Freitag, B., Kujawa, S., Mul, P.M. et al. (2005). Breaking the spherical and chromatic aberration barrier in transmission electron microscopy. *Ultramicroscopy* 102 (3): 209–214.

10 Kabius, B., Hartel, P., Haider, M. et al. (2009). First application of C_c-corrected imaging for high-resolution and energy-filtered TEM. *Journal of Electron Microscopy* 58 (3): 147–155.

11 Levin, B.D.A. (2021). Direct detectors and their applications in electron microscopy for materials science. *Journal of Physics: Materials* 4 (4): 042005.

12 Li, X., Mooney, P., Zheng, S. et al. (2013). Electron counting and beam-induced motion correction enable near-atomic-resolution single-particle cryo-EM. *Nature Methods* 10 (6): 584–590.

13 McMullan, G., Faruqi, A.R., Clare, D., and Henderson, R. (2014). Comparison of optimal performance at 300 keV of three direct electron detectors for use in low dose electron microscopy. *Ultramicroscopy* 147: 156–163.

14 Tietz, H.R. (2008). Design and characterization of 64 MegaPixel Fiber optic coupled CMOS detector for transmission electron microscopy. *Microscopy and Microanalysis* 14 (S2): 804–805.

15 Tate, M.W., Purohit, P., Chamberlain, D. et al. (2016). High dynamic range pixel array detector for scanning transmission electron microscopy. *Microscopy and Microanalysis* 22 (1): 237–249.

16 Zhu, W., Winterstein, J.P., Yang, W.-C.D. et al. (2017). In situ atomic-scale probing of the reduction dynamics of two-dimensional Fe_2O_3 nanostructures. *ACS Nano* 11 (1): 656–664.

17 Armigliato, A., Balboni, R., Carnevale, G.P. et al. (2003). Application of convergent beam electron diffraction to two-dimensional strain mapping in silicon devices. *Applied Physics Letters* 82 (13): 2172–2174.

18 Ozdol, V.B., Gammer, C., Jin, X.G. et al. (2015). Strain mapping at nanometer resolution using advanced nano-beam electron diffraction. *Applied Physics Letters* 106 (25): 253107.

19 Pekin, T.C., Gammer, C., Ciston, J. et al. (2017). Optimizing disk registration algorithms for nanobeam electron diffraction strain mapping. *Ultramicroscopy* 176: 170–176.

20 Zuo, J.M. and Spence, J.C.H. (1992). *Electron Microdiffraction*. New York: Springer US: 358 pages.

21 Zuo, J.M. and Spence, J.C.H. (1993). Coherent electron nanodiffraction from perfect and imperfect crystals. *Philosophical Magazine A* 68 (5): 1055–1078.

22 Zuo, J.M., Vartanyants, I., Gao, M. et al. (2003). Atomic resolution imaging of a carbon nanotube from diffraction intensities. *Science* 300 (5624): 1419–1421.

23 Schlossmacher, P., Burke, M.G., Haigh, S.J., and Kulzick, M.A. (2010). Enhanced detection sensitivity with a new windowless XEDS system for AEM based on silicon drift detector technology. *Microscopy Today* 18 (4): 14–20.

24 Zaluzec, N.J., Burke, M.G., Haigh, S.J., and Kulzick, M.A. (2014). X-ray energy-dispersive spectrometry during in situ liquid cell studies using an analytical electron microscope. *Microscopy and Microanalysis* 20 (2): 323–329.

25 Rez, P., Bruley, J., Brohan, P. et al. (1995). Review of methods for calculating near-edge structure. *Ultramicroscopy* 59: 159–167.

26 Sharma, R., Crozier, P.A., Kang, Z.C., and Eyring, L. (2004). Observation of dynamic nanostructural and nanochemical changes in ceria-based catalysts during *in situ* reduction. *Philosophical Magazine* 84: 2731–2747.

27 Egerton, R.F. (2014). *Electron Energy-Loss Spectroscopy in the Electron Microscope*, 3e. Boston, MA: Springer: 503 pages.

28 Varela, M., Oxley, M.P., Luo, W. et al. (2009). Atomic-resolution imaging of oxidation states in manganites. *Physical Review B* 79 (8): 085117.

29 Mecklenburg, M., Hubbard, W.A., White, E. et al. (2015). Nanoscale temperature mapping in operating microelectronic devices. *Science* 347 (6222): 629–632.

30 Taverna, D., Kociak, M., Stéphan, O. et al. (2008). Probing physical properties of confined fluids within individual nanobubbles. *Physical Review Letters* 100 (3): 035301.

31 Jeanguillaume, C. and Colliex, C. (1989). Spectrum-image: the next step in EELS digital acquisition and processing. *Ultramicroscopy* 28 (1): 252–257.

32 Hunt, J.A. and Williams, D.B. (1991). Electron energy-loss spectrum-imaging. *Ultramicroscopy* 38 (1): 47–73.

33 McVitie, S., McGrouther, D., McFadzean, S. et al. (2015). Aberration corrected Lorentz scanning transmission electron microscopy. *Ultramicroscopy* 152: 57–62.

34 Phatak, C., Petford-Long, A.K., and De Graef, M. (2016). Recent advances in Lorentz microscopy. *Current Opinion in Solid State and Materials Science* 20 (2): 107–114.

35 Zwek, J. (2012). Lorentz microscopy. In: *In-Situ Electron Microscopy: Applications in Physics, Chemistry and Materials Science* (ed. G. Dehm, J.M. Howe and J. Zweck), 347–369. Federal Republic of Germany: Wiley-VCH.

36 Gao, H., Zhang, T., Zhang, Y. et al. (2020). Ellipsoidal magnetite nanoparticles: a new member of the magnetic-vortex nanoparticles family for efficient magnetic hyperthermia. *Journal of Materials Chemistry B* 8 (3): 515–522.

37 Yu, X., JP, D.G., Hara, Y. et al. (2013). Observation of the magnetic skyrmion lattice in a MnSi nanowire by Lorentz TEM. *Nano Letters* 13 (8): 3755–3759.

38 Tanase, M. and Petford-Long, A.K. (2009). In situ TEM observation of magnetic materials. *Microscopy Research and Technique* 72 (3): 187–196.

39 Yu, X. (2019). Imaging magnetic vortices including skyrmions by Lorentz TEM and differential phase-contrast microscopy. *Microscopy and Microanalysis* 25 (S2): 28–29.

40 Peng, L.-c., Zhang, Y., Zuo, S.-L. et al. (2018). Lorentz transmission electron microscopy studies on topological magnetic domains. *Chinese Physics B* 27 (6): 066802.

41 Petford-Long, A.K. and Chapman, J.N. Lorentz microscopy. In: *Magnetic Microscopy of Nanostructures* (ed. H. Hopster and H.P. Oepen), 67–85. Berlin, Heidelberg: Springer-Verlag.

42 Graef, M.D., Willard, M.A., McHenry, M.E. et al. (2001). In-situ Lorentz TEM cooling study of magnetic domain configurations in Ni_2MnGa. *IEEE Transactions on Magnetics* 37 (4): 2663–2665.

43 Budruk, A., Phatak, C., Petford-Long, A.K. et al. (2011). In situ Lorentz TEM magnetization studies on a Fe–Pd–Co martensitic alloy. *Acta Materialia* 59 (17): 6646–6657.

44 Zak, A.M. and Dudzinski, W. (2020). Microstructural and in situ Lorentz TEM domain characterization of as-quenched and γ′-precipitated $Co_{49}Ni_{30}Ga_{21}$ monocrystal. *Crystals* 10 (3): 153.

45 Kim, J.J., Park, H.S., Shindo, D. et al. (2006). *In situ* observations of magnetization process in alnico magnets by electron holography and Lorentz microscopy. *Materials Transactions* 47 (3): 907–912.

46 Wang, A., Chen, F.R., Van Aert, S., and Van Dyck, D. (2010). Direct structure inversion from exit waves: Part I: Theory and simulations. *Ultramicroscopy* 110 (5): 527–534.

47 Cowley, J.M. (1992). Twenty forms of electron holography. *Ultramicroscopy* 41: 335–348.

48 Vincent, R. (2002). Phase retrieval in TEM using Fresnel images. *Ultramicroscopy* 90 (2): 135–151.

49 Chen, F.R., Van Dyck, D., and Kisielowski, C. (2016). In-line three-dimensional holography of nanocrystalline objects at atomic resolution. *Nature Communications* 7 (1): 10603.

50 Yu, Y., Zhang, D., Kisielowski, C. et al. (2016). Atomic resolution imaging of halide perovskites. *Nano Letters* 16 (12): 7530–7535.

51 Gabor, D. and Bragg, W.L. (1949). Microscopy by reconstructed wave-fronts. *Proceedings of the Royal Society of London. Series A. Mathematical and Physical Sciences* 197 (1051): 454–487.

52 Lichte, H. and Lehmann, M. (2007). Electron holography—basics and applications. *Reports on Progress in Physics* 71 (1): 016102.

53 McCartney, M.R., Dunin-Borkowski, R.E., and Smith, D.J. (2005). Electron holography of magnetic nanostructures. In: *Magnetic Microscopy of Nanostructures* (ed. H. Hopster and H.P. Oepen), 87–107. Berlin, Heidelberg: Springer-Verlag.

54 Lehmann, M. and Lichte, H. (2002). Tutorial on off-axis electron holography. *Microscopy and Microanalysis* 8 (6): 447–466.

55 Midgley, P.A. (2001). An introduction to off-axis electron holography. *Micron* 32 (2): 167–184.

56 Jia, C.-J., Sun, L.-D., Luo, F. et al. (2008). Large-scale synthesis of single-crystalline iron oxide magnetic nanorings. *Journal of the American Chemical Society* 130 (50): 16968–16977.

57 Hÿtch, M., Houdellier, F., Hüe, F. et al. (2008). Nanoscale holographic interferometry for strain measurements in electronic devices. *Nature* 453 (7198): 1086–1089.

58 Dunin-Borkowski, R.E., MR, M.C., Frankel, R.B. et al. (1998). Magnetic microstructure of magnetotactic bacteria by electron holography. *Science* 282 (5395): 1868–1870.

59 Harrison, R.J., Dunin-Borkowski, R.E., and Putnis, A. (2002). Direct imaging of nanoscale magnetic interactions in minerals. *Proceedings of the National Academy of Sciences* 99 (26): 16556.

60 Zewail, A.H. (2006). 4D ultrafast electron diffraction, crystallography, and microscopy. *Annual Review of Physical Chemistry* 57 (1): 65–103.

61 Barwick, B., Park Hyun, S., Kwon, O.-H., and Baskin, J.S. (2008). 4D imaging of transient structures and morphologies in ultrafast electron microscopy. *Science* 322 (5905): 1227–1231.

62 LaGrange, T., Armstrong, M.R., Boyden, K. et al. (2006). Single-shot dynamic transmission electron microscopy. *Applied Physics Letters* 89 (4): 044105.

63 King, W.E., Campbell, G.H., Frank, A. et al. (2005). Ultrafast electron microscopy in materials science, biology, and chemistry. *Journal of Applied Physics* 97 (11): 111101.

64 Montgomery, E., Leonhardt, D., and Roehling, J. (2021). Ultrafast transmission electron microscopy: techniques and applications. *Microscopy Today* 29 (5): 46–54.

65 Lobastov, V.A., Srinivasan, R., and Zewail, A.H. (2005). Four-dimensional ultrafast electron microscopy. *Proceedings of the National Academy of Sciences of the United States of America* 102 (20): 7069.

66 LaGrange, T., Campbell, G.H., Reed, B.W. et al. (2008). Nanosecond time-resolved investigations using the in situ of dynamic transmission electron microscope (DTEM). *Ultramicroscopy* 108 (11): 1441–1449.

67 Taheri, M., Lagrange, T., Reed, B. et al. (2009). Laser-based in situ techniques: novel methods for generating extreme conditions in TEM samples. *Microscopy Research and Technique* 72 (3): 122–130.

68 Browning, N.D., Bonds, M.A., Campbell, G.H. et al. (2012). Recent developments in dynamic transmission electron microscopy. *Current Opinion in Solid State and Materials Science* 16 (1): 23–30.

69 Jing, C., Zhu, Y., Liu, A. et al. (2019). Tunable electron beam pulser for picoseconds stroboscopic microscopy in transmission electron microscopes. *Ultramicroscopy* 207: 112829.

70 Lau, J.W., Schliep, K.B., Katz, M.B. et al. (2020). Laser-free GHz stroboscopic transmission electron microscope: components, system integration,

and practical considerations for pump–probe measurements. *Review of Scientific Instruments* 91 (2): 021301.

71 Soer, W.A. and De Hosson, J.T. (2008). In-situ transmission electron microscopy: nanointendation and straining experiments. In: *In-Situ Electron Microscopy and High Resolution* (ed. F. Banhart), 115–160. Singapore: World Scientific.

72 Spiecker, E., Oh, S.H., Shan, Z.-W. et al. (2019). Insights into fundamental deformation processes from advanced in situ transmission electron microscopy. *MRS Bulletin* 44 (6): 443–449.

73 Yu, Q., Legros, M., and Minor, A.M. (2015). In situ TEM nanomechanics. *MRS Bulletin* 40 (1): 62–70.

74 Zhang, J., Ishizuka, K., Tomitori, M. et al. (2020). Atomic scale mechanics explored by in situ transmission electron microscopy with a quartz length-extension resonator as a force sensor. *Nanotechnology* 31 (20): 205706.

75 Bobji, M.S., Pethica, J.B., and Inkson, B.J. (2005). Indentation mechanics of Cu–Be quantified by an in situ transmission electron microscopy mechanical probe. *Journal of Materials Research* 20: 2726–2732.

76 Dehm, G., Legros, M., and Kiener, D. (2012). In-situ TEM straining experiments: recent Progress in stages and small scale mechanics. In: *In-Situ Electron Microscopy: Applications in Physics, Chemistry and Materials Science* (ed. G. Dehm, J.M. Howe and J. Zweck), 227–254. Federal Republic of Germany: Wiley-VCH.

77 Gouldstone, A., Chollacoop, N., Dao, M. et al. (2007). Indentation across size scales and disciplines: recent developments in experimentation and modeling. *Acta Materialia* 55 (12): 4015–4039.

78 Minor, A.M. (2012). In-situ nanoindentation in the transmission electron microscope. In: *In-Situ Electron Microscopy: Applications in Physics, Chemistry and Materials Science* (ed. G. Dehm, J.M. Howe and J. Zweck), 255–277. Federal Republic of Germany: Wiley-VCH.

79 Tanji, T. (2005). Imaging magnetic structures using TEM. In: *Handbook of Microscopy for Nanotechnology II* (ed. N. Yao and Z.L. Wang), 361–394. Boston: Kluwer Academic Publishers.

80 Ishizuka, K., Tomitori, M., Arai, T., and Oshima, Y. (2020). Mechanical analysis of gold nanocontacts during stretching using an in-situ transmission electron microscope equipped with a force sensor. *Applied Physics Express* 13 (2): 025001.

81 Zheng, H., Wang, J., Huang, J.Y. et al. (2012). In situ visualization of birth and annihilation of grain boundaries in an Au nanocrystal. *Physical Review Letters* 109 (22): 225501.

82 Hinks, J.A. (2009). A review of transmission electron microscopes with in situ ion irradiation. *Nuclear Instruments and Methods in Physics Research Section B: Beam Interactions with Materials and Atoms* 267 (23): 3652–3662.

83 Birtcher, R.C., Kirk, M.A., Furuya, K. et al. (2005). In situ transmission electron microscopy investigation of radiation effects. *Journal of Materials Research* 20 (7): 1654–1683.

84 Greaves, G., Mir, A.H., Harrison, R.W. et al. (2019). New microscope and ion accelerators for materials investigations (MIAMI-2) system at the University of Huddersfield. *Nuclear Instruments and Methods in Physics Research Section A: Accelerators, Spectrometers, Detectors and Associated Equipment* 931: 37–43.

85 Tang, B., Zhang, J., Ma, R. et al. (2014). A triple beam *in-situ* facility at Xiamen University. *Materials Transactions* 55 (3): 410–412.

86 Gentils, A. and Cabet, C. (2019). Investigating radiation damage in nuclear energy materials using JANNuS multiple ion beams. *Nuclear Instruments and Methods in Physics Research Section B: Beam Interactions with Materials and Atoms* 447: 107–112.

87 Toader, O., Naab, F., Uberseder, E. et al. (2017). Technical aspects of delivering simultaneous dual and triple ion beams to a target at the Michigan Ion Beam laboratory. *Physics Procedia* 90: 385–390.

88 Hattar, K., Bufford, D.C., and Buller, D.L. (2014). Concurrent in situ ion irradiation transmission electron microscope. *Nuclear Instruments and Methods in Physics Research Section B: Beam Interactions with Materials and Atoms* 338: 56–65.

89 Lian, J., Wang, L.M., Sun, K., and Ewing, R.C. (2009). In situ TEM of radiation effects in complex ceramics. *Microscopy Research and Technique* 72 (3): 165–181.

90 Kirk, M., Baldo, P., Liu, A.Y. et al. (2009). In situ transmission electron microscopy and ion irradiation of ferritic materials. *Microscopy Research and Technique* 72 (3): 182–186.

91 Schäublin, R., Décamps, B., Prokhodtseva, A., and Löffler, J.F. (2017). On the origin of primary ½ a_0 <111> and a_0 <100> loops in irradiated Fe(Cr) alloys. *Acta Materialia* 133: 427–439.

92 Moine, P., Rivieri, J.P., Ruault, M.O. et al. (1985). In situ TEM study of martensitic NiTi amorphization by Ni ion implantation. *Nuclear Instruments and Methods in Physics Research Section B: Beam Interactions with Materials and Atoms* 7-8: 20–25.

93 Meldrum, A., Boatner, L.A., Weber, W.J., and Ewing, R.C. (2002). Amorphization and recrystallization of the ABO_3 oxides. *Journal of Nuclear Materials* 300 (2): 242–254.

94 Johnson, E., Touboltsev, V.S., Johansen, A. et al. (1997). TEM and RBS/channelling of nanosized bicrystalline (Pb, Cd) inclusions in Al made by sequential ion implantation. *Nuclear Instruments and Methods in Physics Research Section B: Beam Interactions with Materials and Atoms* 127–128: 727–733.

95 Liu, L.Z.-Y., McAleese, C., Sridhara Rao, D.V. et al. (2012). Electron holography of an in-situ biased GaN-based LED. *Physica Status Solidi C* 9 (3–4): 704–707.

96 Tan, X. (2012). In-situ TEM with electrical bias on ferroelectric oxides. In: *In-Situ Electron Microscopy: Applications in Physics, Chemistry and Materials Science* (ed. G. Dehm, J.M. Howe and J. Zweck), 321–346. Federal Republic of Germany: Wiley-VCH.

97 Möller, M., Gaida, J.H., Schäfer, S., and Ropers, C. (2020). Few-nm tracking of current-driven magnetic vortex orbits using ultrafast Lorentz microscopy. *Communications on Physics* 3 (1): 36.

98 Spolenak, R. (2012). Current-induced transport: electromigration. In: *In-Situ Electron Microscopy: Applications in Physics, Chemistry and Materials Science* (ed. G. Dehm, J.M. Howe and J. Zweck), 281–301. Federal Republic of Germany: Wiley-VCH.

99 Fujii, T., Arita, M., Hamada, K. et al. (2011). *I–V* measurement of NiO nanoregion during observation by transmission electron microscopy. *Journal of Applied Physics* 109 (5): 053702.

100 Hirose, R., Arita, M., Hamada, K. et al. (2005). In situ conductance measurement of a limited number of nanoparticles during transmission electron microscopy observation. *Japanese Journal of Applied Physics* 44 (24): L790–L792.

101 Takahashi, Y., Kudo M, Fujiwara I et al. (2015). Visualization of conductive filament during write and erase cycles on nanometer-scale ReRAM achieved by in-situ TEM. *2015 IEEE International Memory Workshop (IMW)*, Monterey, CA (17-20 May 2015). https://ieeexplore.ieee.org/document/7150312.

102 Lu, X., Adkins, E.R., He, Y. et al. (2016). Germanium as a sodium ion battery material: in situ TEM reveals fast sodiation kinetics with high capacity. *Chemistry of Materials* 28 (4): 1236–1242.

103 Cheng, Y., Zhang, L., Zhang, Q. et al. (2021). Understanding all solid-state lithium batteries through in situ transmission electron microscopy. *Materials Today* 42: 137–161.

104 Xu, T.T., Ning, Z.Y., Shi, T.W. et al. (2014). A platform for in-situ multi-probe electronic measurements and modification of nanodevices inside a transmission electron microscope. *Nanotechnology* 25 (22): 225702.

105 Li, L., Jokisaari, J.R., and Pan, X. (2015). In situ electron microscopy of ferroelectric domains. *MRS Bulletin* 40 (1): 53–61.

106 Budruk, A., Phatak, C., Petford-Long, A.K., and De Graef, M. (2011). In situ Lorentz TEM magnetization study of a Ni–Mn–Ga ferromagnetic shape memory alloy. *Acta Materialia* 59 (12): 4895–4906.

107 Dunin-Borkowski, R.E., MR, M.C., Kardynal, B. et al. (2000). Off-axis electron holography of patterned magnetic nanostructures. *Journal of Microscopy* 200 (Pt 3): 187–205.

108 Yano, T., Murakami, Y., Kainuma, R., and Shindo, D. (2007). Interaction between magnetic domain walls and antiphase boundaries in $Ni_2Mn(Al,Ga)$ studied by electron holography and Lorentz microscopy. *Materials Transactions* 48 (10): 2636–2641.

109 Volkov, V.V. and Zhu, Y. (2000). Dynamic magnetization observations and reversal mechanisms of sintered and die-upset Nd–Fe–B magnets. *Journal of Magnetism and Magnetic Materials* 214 (3): 204–216.

110 Rodríguez, L.A., Magén, C., Snoeck, E. et al. (2013). Quantitative in situ magnetization reversal studies in Lorentz microscopy and electron holography. *Ultramicroscopy* 134: 144–154.

111 Arita, M., Tokuda, R., Hamada, K., and Takahashi, Y. (2014). Development of TEM holder generating in-plane magnetic field used for in-situ TEM observation. *Materials Transactions* 55 (3): 403–409.

112 Dietrich, C., Hertel, R., Huber, M. et al. (2008). Influence of perpendicular magnetic fields on the domain structure of permalloy microstructures grown on thin membranes. *Physical Review B* 77 (17): 174427.

113 Inoue, M., Tomita, T., Naruse, M. et al. (2006). Development of a magnetizing stage for in situ observations with electron holography and Lorentz microscopy. *Journal of Electron Microscopy* 54 (6): 509–513.

114 Masseboeuf, A., Gatel, C., Bayle-Guillemaud, P. et al. (2009). The use of Lorentz microscopy for the determination of magnetic reversal mechanism of exchange-biased $Co_{30}Fe_{70}$/NiMn bilayer. *Journal of Magnetism and Magnetic Materials* 321 (19): 3080–3083.

115 Kryshtal, A., Mielczarek, M., and Pawlak, J. (2022). Effect of electron beam irradiation on the temperature of single AuGe nanoparticles in a TEM. *Ultramicroscopy* 233: 113459.

116 Zheng, H. and Zhu, Y. (2017). Perspectives on in situ electron microscopy. *Ultramicroscopy* 180: 188–196.

117 Peng, L., Zhang, Y., Ke, L. et al. (2018). Relaxation dynamics of zero-field skyrmions over a wide temperature range. *Nano Letters* 18 (12): 7777–7783.

118 Ding, B., Li, Z., Xu, G. et al. (2020). Observation of magnetic skyrmion bubbles in a van der Waals ferromagnet Fe_3GeTe_2. *Nano Letters* 20 (2): 868–873.

119 Jiang, W., Zhang, S., Wang, X. et al. (2019). Quantifying chiral exchange interaction for Néel-type skyrmions via Lorentz transmission electron microscopy. *Physical Review B* 99 (10): 104402.